

THE OXIDATION AND SUBLIMATION OF GRAPHITE  
IN SIMULATED RE-ENTRY ENVIRONMENTS

J. W. Metzger  
M. J. Engel  
N. S. Diaconis

Space Sciences Laboratory  
General Electric Company  
Philadelphia, Pa.

N66-22255

FACILITY FORM 802

(ACCESSION NUMBER)	(THRU)
91	1
(PAGES)	(CODE)
CR 60395	18
(NASA CR OR TMX OR AD NUMBER)	(CATEGORY)

To be presented at 18th Annual Meeting of Heat Transfer  
and Fluid Mechanics Institute, Los Angeles, California  
June 21-23, 1965

This work was supported by the Space Nuclear Propulsion  
Office of NASA/AEC under Contract SNPC-10 and the  
U.S. Air Force Ballistic Systems Division under Contract  
AF 04 (694)-222

GPO PRICE \$ \_\_\_\_\_  
CFSTI PRICE(S) \$ \_\_\_\_\_


Hard copy (HC) 3.00  
Microfiche (MF) .75

NASA CR #60395

## INTRODUCTION

As the state of the art of re-entry vehicle technology continues to advance the demands placed upon thermal protection systems for proposed missions become increasingly more severe. Whereas early designs in general incorporated plastics and re-inforced plastics as the ablative heat protection material, more recently the designer has given serious consideration to refractory materials for such applications. Certainly interesting candidates in this area are the graphites and many of the carbonaceous alloys.

While the choice of a vehicle heat shield material involves the consideration of many aspects of design requirements bearing on structural, fabrication, thermodynamic and signature criteria, in this paper we will concern ourselves only with the material thermochemical response to the re-entry environment. Although there are many types of graphitic materials, the choice to study a particular composition does not significantly compromise the investigation. Theoretical treatments in the literature (5, 6, 9, 10, 11) consider basically a carbon matrix and to this extent most graphites per se should be covered by such analyses. In this paper in which we will describe an experimental study of the oxidation and sublimation of such materials we will deal specifically with two types of graphite. These are ATJ, a fine grain commercial graphite produced by the National Carbon Company which has found application in numerous aerospace ventures and pyrolytic graphite, a highly anisotropic material produced by vapor deposition.



The information presented herein is a report of the current status of the study of graphite degradation in re-entry environments that has been in progress for a number of years at the Space Sciences Laboratory of the General Electric Co. An earlier report (ref. 8) presented some preliminary results on ATJ oxidation. The oxidation study which is now greatly augmented, and results of graphite performance while undergoing sublimation are the subject of this release. The experimental program is described, the data analysis techniques used to obtain the various correlations are presented and the comparison of the results with the theoretical treatments of Scala are shown.

## TECHNICAL APPROACH

### 1. Test Facilities

To obtain data over the broad range of temperature of interest in this study it was necessary to conduct the test program in more than one test facility. The major portion of the testing was conducted in a hypersonic arc tunnel in which environments were established for obtaining the rate controlled and diffusion controlled results (as defined by ref. 5). To obtain data in the sublimation regime a free jet arc facility was used.

All tests for the study of ATJ Graphite were conducted in the SSL Hypersonic Arc Tunnel. This system is comprised of a tandem Gerdien arc heater, a conical nozzle through which the heated test gas is expanded into a continuously evacuated test section where the specimens are normally mounted, a diffuser aft of the test section, and a high speed mechanical vacuum pump. The tunnel is illustrated in Figure 1 and the arc heater in Figure 2.

The heater arrangement (Figure 2) is such that air is admitted tangentially to each Gerdien unit through vortex chambers located between the electrode housings and the plenum chamber. Valving in the air system provides a method of dividing the incoming air flows into two portions which are subject to close control. The greater portion of the air is bled from the system through exhaust ports in the electrode housings. In the course of its passage from the inlets to exhaust ports, the exhaust air carries with it the carbon products produced from

the graphite electrodes which would normally contaminate the test gas. The remaining portions of the air admitted (which constitute the test gas) pass into the plenum from both sides, acquiring additional energy from the arc column. Contaminants, measured spectroscopically, constitute less than 100 parts per million of the test gas. The rotation induced in the air as it is admitted tangentially, is oppositely directed in the two halves of the arc, the opposed rotations tending to offset one another as the two flows enter the plenum and mix. The combined flow then passes from the plenum through the throat of the conical nozzle.

The nozzle is constructed in two parts, one of which is essentially an extension of the other. The up-stream section has an exit diameter of 1.2", while the extension, when added to the short nozzle, provides a nozzle of 5" exit diameter. All parts of the arc hardware and the nozzle are cooled with pressurized high velocity water in order to provide them with maximum service life.

The free jet facility used for the higher temperature testing is shown in Figures 3a and 3b. The major difference between this unit and the design used for the arc tunnel is in the plenum chamber, the basic shape of which has been changed from a large cylindrical section to a small tee section. Whereas the former plenum diameter was 3 to 4 times the diameter of the vortex chamber constricting orifices, the orifice and plenum diameters in the present unit are equal. With this arrangement the stay time in the column

and plenum regions, and consequently the energy losses of the test gas, are significantly reduced. Test flows are sub-sonic and the model is located only a short distance downstream of the arc column in rather high stagnation enthalpy flows. Details of this facility and the arc tunnel can be found in Ref. 1 & 2 respectively. Whereas the ATJ studies were performed in the arc tunnel, only pyrolytic graphite testing was performed in the free jet.

## 2. Test Procedure

To measure the enthalpy of the test gas, a total calorimeter was used. This device (Figure 4) used in the arc tunnel consists of a cylindrical housing containing a labyrinth passage for the test gases. The adjacent walls are cooled with pressurized water to remove the heat transferred from the test gas. The calorimeter is affixed directly to the throat of the nozzle, located in the wall of the arc heater plenum. The heated test gas from the plenum is directed through the calorimeter where it transfers the bulk of this energy to the circulating water. The heat remaining in the gas as it leaves the calorimeter is monitored by a thermocouple and its mass flow rate is measured. Similarly, the temperature rise and mass flow of the circulating water are measured continuously during a test. Several thermocouples are mounted in the copper structure of the calorimeter to evaluate the heat "stored" in the walls. The test is continued until all reporting thermocouples equilibrate. The evaluation of the reported data, essentially a heat balance between the calorimeter elements and the test gas, results in a measure of the total heat content of the gas. Since it is estimated that there are some minor heat losses

which cannot be evaluated, the value of the enthalpy obtained will be slightly conservative. It should further be noted that the enthalpy determined is a "mean" of the distribution of energy across the jet; other measurements performed with a spectrograph also indicate enthalpy variations across the jet. In general these spectrographic measurements have recorded enthalpies about 6 percent higher than those obtained by total calorimetry.

Total calorimeter data were also obtained in the free jet facility using a similar approach to that used in the arc tunnel. The only difference involved the use of an adapter that fit into the test chamber to collect the test gases. This arrangement is shown in Figure 5.

Model measurements as part of the test program consisted of surface pressure, surface heat transfer and specimen surface temperature. The pressure values were obtained with pilot probes while the heat transfer was measured with transient calorimeter models corresponding to each of the test specimen configurations. A typical model calorimeter is shown in Figure 6. The calorimeter bodies were constructed from phenolic nylon, chosen for its low thermal conductivity and into each of these, a copper cylinder was inserted. A thermocouple attached to the back face of the copper slug recorded the rise in temperature in the copper during exposure. By confining the slug within a poor thermal conductor, the heat transfer rate was evaluated on the basis of a one-dimensional heat flow analysis although first order corrections for the heat loss from the slug were incorporated. One inch specimens were equipped with 1/4" diameter slugs while 1/4" bodies employed 1/8" diameter slugs.

To obtain heat transfer to a 1/16" diameter specimen, a rigid 60 mil copper rod was employed, and to minimize lateral heat input, the rod was coated with a 2 to 3 mil layer of RTV silicone rubber (a good thermal insulating material). The 1/16" calorimeter appeared to perform extremely well, but in order to provide a higher level of confidence in this technique, several calorimeters constructed from 1/4" diameter copper rod coated with a correspondingly thin RTV skin were tested. Results were closely comparable to the data obtained from the 1/4" phenolic nylon cylinders with 1/8" diameter copper inserts.

Several sizes of cylindrical specimens were involved in the acquisition of mass rate data. Sizes included diameters of 1/16", 1/4", 3/4" and 1". The configurations and dimensions of the specimens are shown in Figure 7a and 7b.

During the course of the arc tunnel program, various circumstances arose which warranted the introduction of several modifications to the specimens. Variations were introduced principally to the 1/4" diameter cylinders. It was found that during consecutive tests the surface temperatures of similarly constructed models equilibrated at temperatures that differed but little from one another. The results were thus confined to a relatively narrow range of temperatures. In order to extend the temperature range, variations of test specimens retaining the basic 1/4" diameter cylindrical shape were constructed (Figure 7c). Objectives sought by making such changes were (a) the alteration of the thermal conduction paths and (b) a change in the



heat storage volume for the specimen adjacent to the exposed surface. While the modified specimens did provide an increase in the range of surface temperatures obtained, the effects were not as pronounced as expected. However, for the same reasons, the 1/16" specimens were also tested in one other configuration (Figure 7b) in addition to the original. In this case, the increase in temperature range was also relatively small.

Measurements of surface temperature were made for each specimen while undergoing test. These were obtained with a recording two-color pyrometer employing two phototubes with maximum responses at different wavelengths. One tube has maximum response in the red portion of the spectrum, the other in the blue. The evaluation of the relative responses of the two tubes is interpreted as a color temperature. For models tested in the flow from the 5" diameter nozzle, the two color pyrometer views the specimens through a test section window. When the 1.2" diameter nozzle is employed, use is made of a special small port built into the arc heater mounting flange.

In the case of free jet testing, determination of surface temperature histories in general involved observing the test surface through both the ablation products and the high enthalpy air flows. As a check on the pyrometer measurements, model surface temperatures were also obtained by spectrographic means. Whenever extraneous radiators appeared in the pyrometer band width the spectrographic data were analyzed to determine temperature values.

## TEST RESULTS

### 1. Calorimeter Measurements

Total enthalpy of the test gas was measured for each of the two enthalpy levels at which the arc tunnel was operated and the results of the tests, using the total calorimeter have been summarized in Table 1. The evaluation process for data acquired from the calorimeter is a heat balance between a heat exchanger (the calorimeter) and the test fluid (air) after the system has reached steady state operation. Similar data for the free jet are presented in Figure 8 as a function of distance from the arc column of the heater. Model heat transfer results are shown in Figure 2.

### 2. Specimen Mass Loss

The mass loss data obtained from the cylindrical test specimens consisted of the difference in length resulting from exposure to the test environment. The differences were obtained from micrometer measurements taken before and after test. Length change at the stagnation point was used in preference to measured mass loss because it was not feasible to give accurate consideration to mass lost from the side wall of the cylinder. In the tunnel tests (where test times were quite long) the gross mass lost from a cylinder varied between two and three times the mass lost at the stagnation region of the specimen, as calculated from the length change using the following expression:  $\Delta m = \rho A (\Delta \ell)$ .

It is possible that some mass is driven from below the receding face of a specimen. Hence a comparative evaluation of mass rate based on length change and on mass loss over an area with protected side walls would be informative.

Provision for such a comparison was made on the one inch diameter specimens tested during the program. Since the diameter was sufficient, a small insert (1/4" diameter) was press fitted into a centerline cavity in the one inch specimens. Comparison of the results from weight and length measurements showed the weight loss generally to be about 5% greater.

A few specimens showed a measurable decrease in diameter as a result of side wall mass losses. This was especially noticed on the 1/16" diameter models. The net effect of such diametral decrease is a tendency for the heat transfer rate at the stagnation point to increase slightly ( $\dot{q}_0 \propto 1/\sqrt{R}$ ). Hence, mass rates for the longer run times might be expected to be slightly larger. Data from the various runs in the tunnel are shown in Tables 3 to 8, and free jet results are indicated in Fig. 9.

### 3. Rate of Mass Loss

In order to present the results of the tests in a form comparable to the theoretical representation, it is necessary to obtain the mass rate of oxidation for incremental temperatures. While it may be possible in theory to evaluate mass rate as a continuous function of surface temperature from motion film records of the tests and time resolved surface temperature recordings, the relatively small dimensional change in the specimen puts a prohibitive penalty on the accuracy attainable. The technique used in this program employed a system of length and time differences.

Specimens were exposed to the test environment for various intervals of time, resulting in incremental differences in length change. The calculation of rate of mass loss per unit area proceeded from taking differences between length losses and times among the various specimens in the following manner:

$$\dot{m}_w = \rho \left( \frac{\Delta l_2}{\Delta t_2} - \frac{\Delta l_1}{\Delta t_1} \right)$$

The calculated mass loss rate is considered to represent that existing at the average temperature for the two test points evaluated, i.e.:  $(T_1 + T_2)/2$ .

Results are shown in Table 3 to 8 and Fig. 17.

#### 4. Surface Temperature

Typical surface temperature histories of specimens run in the arc tunnel obtained from the pyrometer measurements are shown in Figure 10. An example of similar measurements in the free jet are presented in Figure 9. Details of the data reduction techniques are available in Ref. 1 and 2.

## DISCUSSION OF RESULTS

### 1. Test Environments

While the basic objective of the investigation was to establish the performance of the graphite materials over a broad range of surface temperature, the character of flows of electric arc heated facilities injects additional variables into the problem. Because of the high enthalpies generated in such facilities subsequent expansion of the gas in nozzles usually results in non-equilibrium conditions in the test section. In addition the magnitude of the flow properties is such that very low Reynolds number conditions result. As a result when considering the range of model sizes, model pressures and enthalpy values that were involved in this study, local model conditions ranged from continuum to near-free molecular values.

In order to determine the type of simulation performance which the arc tunnel facility could deliver, it was necessary to define the conditions of flow provided at different conditions of operation. Based on facility evaluation tests previously conducted in the Hypersonic Arc Tunnel (Ref. 3), a series of computations were made to determine the Reynolds number at the several test conditions. Although the available spectrographic evidence indicates that the flow is in equilibrium as it leaves the plenum, sufficient evidence also exists that the flow freezes very rapidly in the vicinity of the throat of the nozzle (Ref. 4). Calculation of both the equilibrium and frozen flow expansions through the nozzle according to the treatment in Ref. 3 showed that while the local free

stream properties were quite different at the test locations, the Reynolds number for both frozen and equilibrium flow in the model stagnation region were of approximately the same magnitude. The variation ranged from 8-15% over the spread in Reynolds number. Consequently, when it was necessary to introduce a Reynolds number for tunnel tests, an average value was used for each set of conditions.

For the free jet facility, while higher enthalpy flows are generated, the greatly increased model pressure ( $p_m \sim 1 \text{ atm}$ ) encountered in the subsonic flow field provides the means whereby continuum flow criteria would apply.

## 2. Oxidation of Graphite

Once the numerous mass rate values had been computed (Tables 3-8) they were plotted as a function of reciprocal temperature with the objective of determining the activation energy ( $E$ ) and the reaction rate coefficient ( $k_o$ ) for the equation:

$$\dot{m} = k_o \sqrt{P_e} e^{-E/RT}$$

For pure reaction rate controlled oxidation, the given equation can be rewritten in the form of the integrated Arrhenius equation, which requires that the natural log of  $\dot{m}'$  vs.  $1/T$  shall be a straight line.<sup>1</sup> It was not obvious from the examination of the data plotted in this form (Fig. 11) that this was the case.

---

1. In this report, direct reference to unadjusted mass rate data employs the symbol  $\dot{m}'$ ; corrected data is denoted by the conventional  $\dot{m}$ .

Since it was fully expected that some of the specimens would have been oxidized under conditions of diffusion control a departure from a linear plot was not surprising. The deviation obtained tended to confirm the presence of the diffusion controlled activity. Coupled with the scatter of the data points, the narrow range of mass rates for which linearity might be assumed made it difficult to plot a straight line which could be considered properly representative of the reaction. In lieu of an estimated slope of great uncertainty it was decided that a value would be chosen which was typical for graphite materials. The slope is a measure of the activation energy. Consultation with the available literature led to a choice of 44.0 kilocalories as a good representative value. A straight line with this slope was constructed to pass through the bulk of data points estimated to be predominantly reaction rate controlled. Based on the constructed line, the reaction coefficient was determined:

$$k_o = 4.42 \times 10^5 \text{ lb/sec.ft.}^2 \text{ atm}^{1/2}$$

The equation for the reaction rate oxidation of graphite was then substituted along with the theoretical diffusion controlled oxidation correlation of Ref. 5

$$\dot{m}_D = 6.2 \times 10^{-3} \frac{P_e^{1/2}}{R_B^{1/2}} \frac{\text{lb}}{\text{ft.}^2\text{-sec}}$$

into the transition regime relation presented in Ref. 6

$$\dot{m} = \frac{1}{\left[ \frac{1}{(\dot{m}_R)^2} + \frac{1}{(\dot{m}_D)^2} \right]^{1/2}}$$

Curves were computed for each type specimen and test condition (see Appendix B) and the results are shown in Fig. 11. It is evident that in the diffusion controlled regime (constant mass rate) the data points are high with respect to the theory. Because the test facility provided environments which were characterized by non-continuum flows, these differences were expected.

The theory developed by Scala (Ref. 5) to describe the oxidation of graphite was based on flow of high Reynolds number. In Ref. 2 that theory is extended to regions of low Reynolds number and to molecular flow. The extension provides that data of both rate controlled and diffusion controlled oxidation must be adjusted in order to compare it with high Reynolds number continuum based theory, or vice versa. In their final forms, the modifications consist of applying a Stanton number ratio correction factor to data in the diffusion controlled regime or an effective pressure ratio correction factor to data in the reaction rate controlled regime. Both these factors are functionally dependent upon the Reynolds numbers corresponding to the test flow conditions. From calculated nominal values of Reynolds number per foot, corresponding to the various test conditions, the shock Reynolds number for each model was determined. The appropriate correction factors for either oxidation process were then obtained from the graph of Stanton number ratio vs.  $Re_s$  (Figure 12) or the graph of  $\left[ p_{O_2} / .21 \rho_{\infty} V_{\infty}^2 \right]$  vs.  $Re_s$  (Figure 13). \* Data point values must be divided by the correction factors determined from these graphs.

---

\* Both Fig's. 12 and 13 are reprinted from Ref. 2 where they are Fig's. 22 and 23



In examining the mass rate plotted against  $1/T$ , it may be seen that many of the points lie near the transition region of the theory curves. For these points, correction factors are needed which are intermediate between those appropriate for diffusion control and for rate control. To accomodate these points, the theoretical expressions were examined and the contribution of each factor was weighted for each point in the transition region. Refer to Appendix C. Once the appropriate correction factors were determined for all regions containing data, they were applied, each to its corresponding datum point, to determine the mass rates in terms of Scala's original theory (Tables 3-8).

A second graph of  $\dot{m}$  vs.  $1/T$  was prepared showing the adjusted data over-plotted on the theoretical curves (Figure 14). It may be seen that the diffusion controlled data are decreased and conform reasonably well to the predicted performances. In general, the rate data are increased in value, although the changes in position with respect to the theory curves are less pronounced because of the near-vertical slope of the reaction rate portions of the curves.

It is interesting to note that when the data are corrected, the shift of reaction rate data may be sufficient to warrant the construction of a new, displaced slope for the activation energy and alteration of the weighting factors in the transition region. Extrapolated to its extremity, this becomes an iterative process which ceases when the required degree of accuracy has been attained. In the present case, the scatter of the data points is sufficient to make further approximations unjustified.

Having shown that the mass loss rate data does indicate reasonable concurrence with the theory, the final step was to prepare a plot of the data normalized with respect to pressure and specimen radius. However, it was evident that data corrected to correspond to the theory curves would tend toward a more crowded pattern. In order to better examine the relative correspondence of theory and experiment for the individual test conditions, the theory curves were modified for  $Re_g$  effects as the correction factors indicated, while the original mass rate data were normalized with respect to pressure and body radius only (Tables 3-8). The results were plotted ( $\dot{m}' = \sqrt{R_B/P_e}$  vs  $T_w$ ; Figure 15) to provide a clearer picture of the degree to which theory and experiment agree.

Finally, the appropriate correction factor was applied to each datum point normalized with respect to pressure and specimen radius (Tables 3-8), and the computed results were incorporated into a plot ( $\dot{m}'\sqrt{R_B/P_e}$  vs.  $T_w$ ; Figure 16) in which the theory curves remain in the form calculated from the unmodified continuum theory. The theoretical curves predict a dependency of data on the body size only in the reaction rate controlled regime but independence with respect to both pressure and body size in the diffusion controlled regime. The methods employed in reducing the data are described in detail in Appendix C.

Aside from the scatter of data it may be seen that there is indeed a trend which places the 1/4" specimen data between the majority of one inch and of

1/16" specimen data. In addition, the data for all three model sizes are in approximately the proper relation to one another as predicted by the theory. Note also that the  $6.2 \times 10^{-3} \text{ lb/ft}^{3/2} \text{ sec. atm}^{1/2}$  plateau is placed in the midst of the data points corresponding to diffusion controlled oxidation.

The experimental results assuredly concur with the theory when a mean value of the data is considered.

### 3. Sublimation of Graphite

As mentioned earlier the free jet tests were not conducted with ATJ graphite, but rather with pyrolytic graphite. Even though a different form of graphite is being used the data obtained are characteristic of diffusion controlled and sublimation thermochemical degradation and theoretically this should be independent of the crystalline structure of the material. From the data shown in Fig. 9a and b one can observe the severity of the test environment produced in the free jet. This is indicated by the attainment of sublimation temperature in less than one second (Fig. 9a). Once that plateau is reached, the temperature remains constant for the remainder of the test time. The mass loss data, computed from the change in the length of the specimen at the stagnation point and the density of the material, shows essentially a linear variation with time as expected. The small drop in temperature at the longer times is accompanied by a lower rate of mass loss. These effects are attributed to a reduced heating rate caused by the models becoming slightly concave during a longer run. The low surface temperature during the first second of exposure is responsible for the failure of an extrapolated straight line through the data to go through the origin. Similar results

are shown for the lower enthalpy flow in Fig. 9b. The material again heats up very rapidly except that the level of temperature attained is considerably lower. From the mass rate value the correlation  $\dot{m} \sqrt{R_B/P_e}$  is established and these results are shown in Fig. 17. The three points shown correspond to the mass loss rate lines - best fit and high and low uncertainty limits - shown in Fig. 9. The temperature spread is due to the maximum uncertainty in fitting the experimental spectral intensities to theoretical spectral distributions (temperature determined by spectroscopy).

Before the data can be plotted on Fig. 17, however, the value of  $R_B$  must be chosen. Since the theoretical relations have been developed for a Newtonian pressure distribution on a sphere and the present experiments have been conducted in a subsonic flow on a flat faced cylinder, we must account for this difference in comparing experiment with theory. In essence, an effective radius for an equivalent body in a Newtonian flow field has been established and used to compute the correlation parameter for the experimental data.

The determination of an appropriate value for the effective radius (or the model stagnation point velocity gradient) in a subsonic high enthalpy flow field when the model size is of the order of the test jet is not a straightforward problem. Analyses are available in classical hydrodynamics dealing with the impingement of streams on flat plates and discs; however, there appears to be no satisfactory analytical way to account for interference from the walls of the small test chamber. Also, accurate measurement of surface pressure gradients are extremely difficult in the severe test environments.

Because of these problems, an effective radius was determined by inference from the ATJ data since these have been shown to be in good agreement with the theory in the diffusion controlled regime. It was assumed that the theoretical diffusion controlled mass parameter value  $\left(\dot{m} \sqrt{R_B/P_e}\right)_D$  was also correct for the free jet tests and a radius calculated using the test data. This gave  $R_B = 2.4 R_B \text{ geom.}$

A second experimentally based method can also be used to determine an effective  $R_B$  value. This approach uses the measured stagnation point convective heat transfer and enthalpy values and infers an  $R_B$  value by comparing results with theory. Using the theoretical results of Scala and Baulknight (7) and the nominal test conditions ( $\bar{h} = 490 \text{ RT}_0, P_e = 1 \text{ atmosphere, } \dot{q}_c = 2050 \text{ BTU/ft}^2\text{-sec}$ ) we get  $R_B = 2.9 R_B \text{ geom.}$

These two  $R_B$  values are not greatly different; however, we have used the first value, instead of an average, for two reasons. First, a 21% uncertainty in  $R_B$  is indicative of only about a 10% uncertainty in heating rate. This is no better than should be expected in this type of test environment. Second, the use of an experimental measurement of the same type as that used in obtaining the data of interest (graphite material loss rate) to establish the experimental base for deduction of an effective  $R_B$  eliminates those sources of potential error peculiar to a calorimeter measurement.

The experimental results in Fig. 17 are compared with the sublimation theory of Scala and Gilbert (6). Because of the scatter in the temperature data

(  $\pm$  5%) it was not possible to make a more careful evaluation. Even though the stated temperature variation is within general experimental accuracy, a further improvement will be required due to the extreme sensitivity of material degradation to temperature in the sublimation region. As a general comment however, one might say that the theory and experiment yield comparable results.

## REFERENCES

- 1.) Diaconis, N.S., Weber, H.E., Warren, W.R.; Technique for Severe Radiative and Convective Heating Environments for Materials Evaluation; Pres. 3rd Hyper. Tech. Sym. - March 17-18, 1964 Denver, Col.  
(Also GE MSD TIS R64SD24, March, 1964)
- 2.) M.J. Engel, et al, The Effects of Atmospheric Re-Entry on Graphitic Particles, Final Rept. Contract SNPC-10, SNPO, Cleveland, Ohio, January, 1964
- 3.) Warren, W.R., Diaconis, N.S., Air Arc Simulation of Hypersonic Environments, GE TIS R62SD25, April, 1962, Pres. Int'l Hypersonics Conf. M.I.T., Cambridge, Mass., August, 16-18, 1961.
- 4.) Eschenroeder, A.Q., et al, "Exact Solutions for Non-Equilibrium Expansions of Air With Coupled Chemical Reactions", CAL Rpt. No. AF-1413-A-1, AFO SR 622, May, 1961.
- 5.) Scala, S.M., The Ablation of Graphite in Dissociated Air, Part I, Theory, IAS Paper No. 62-154, Thirtieth Nat'l. Summer Mtg., June 1962 (also GE MSD TIS R62SD72, September, 1962).
- 6.) Scala, S.M. and Gilbert, L.M.; The Sublimation of Graphite at Hypersonic Speeds; GE MSD TIS R64SD55, August, 1964.
- 7.) Scala, S.M. and Baulknight, C.W.; Transport and Thermodynamic Properties In a Hypersonic Laminar Boundary Layer, Part 2, Applications; ARS Journal, Vol. 30, No. 4, pp 329-336, April, 1960.
- 8.) Diaconis, N.S., Gorsuch, P.D. and Sheridan, R.A., The Ablation of Graphite In Dissociated Air, Part 2, Experiment; Pres. Thirtieth IAS Nat'l. Summer Mtg. June, 1962, ( also GE MSD TIS R62SD86, September, 1962).
- 9.) Denison, M.R. and Dooley, D.A.; Combustion In The Laminar Boundary Layer of Chemically Active Sublimators, Aeronutronic Systems Rept. U-110, Sept., 1957.

- 10.) Moore, J.A. and Zlotnick, M.; Combustion of Carbon in An Air Stream, AVCO, RAD-TR-9-60-32, December, 1960.
- 11.) Welsh, W.E., Jr. and Chung, P.M.; A Modified Theory for the Effect of Surface Temperature On the Combustion Rate of Carbon Surfaces In Air, Proc. of 1963 Ht. Trans. and Fluid Mechanics Inst., Calif. Inst. of Tech., Calif., June, 1963 Stanford Univ. Press pp 146-159.



## APPENDIX A

### List of Symbols

ATJ	ATJ grade graphite
C	diffusion-controlled mass transfer constant
$C_H$	Stanton number
E	activation energy
f	distribution function; fractional ratio
$F_m$	mass transfer rate modification factor
$h_s$	stagnation enthalpy
$k_o$	specific reactivity coefficient
$\dot{m}$	mass transfer rate of ablating (or oxidizing material) per unit area
$\dot{m}'$	unadjusted mass transfer rate per unit area
n	number density; reaction order
N	ratio, $\dot{m}_R/\dot{m}_D$
$P_{O_2}$	pressure of oxygen
$P_e$	stagnation pressure
$\dot{q}$	heat transfer rate per unit area
$R_B$	radius of body
Re	Reynolds number
$Re_s$	shock Reynolds number
$RT_o$	enthalpy at ambient conditions (33.86 Btu/lb)
t	time
T	temperature
$\Delta$	difference or change
$\rho$	density

### Subscripts

B. L.	boundary layer
D	diffusion control
eff.	effective
ff	flat face
F. M.	free molecular
H. R.	high Reynolds number
L. R.	low Reynolds number
R	reaction rate control

# UNCLASSIFIED

## APPENDIX B

### DERIVATION OF COMBINED THEORETICAL-EMPIRICAL EQUATIONS

In order to graphically represent the combined theoretical-empirical mass loss performance of the materials studied in this program, the following expressions were employed:

$$\text{Let } \dot{m}_R = k_o \sqrt{P_e} e^{-E/RT} \quad \text{represent rate controlled mass loss} \quad (1)$$

$$\text{Let } \dot{m}_D = C \sqrt{P_e/R_B} \quad \text{represent diffusion controlled mass loss} \quad (2)$$

$$\text{Let } \dot{m} = \frac{1}{\left[ \frac{1}{(\dot{m}_R)^2} + \frac{1}{(\dot{m}_D)^2} \right]^{1/2}} \quad \text{represent transition from rate controlled to diffusion controlled mass loss} \quad (3)$$

Substitution of (1) and (2) into (3) yields, after some algebraic re-arrangement,

$$\dot{m} = \frac{k_o \sqrt{P_e}}{\left[ e^{2E/RT} + \left( \frac{k_o}{C} \right)^2 R_B \right]^{1/2}} \quad (4)$$

from which the curves on Figures 32, 33, 52 and 53 were calculated.

Further, if one lets

$f_1$  = fractional ratio of Stanton No.

$f_2$  = fractional ratio of effective pressure ratio

replacing  $\dot{m}_D$  by  $f_1 \dot{m}_D$  and  $\dot{m}_R$  by  $f_2 \dot{m}_R$  in eq. (3) one may derive

$$\dot{m}' = \frac{f_2 k_o \sqrt{P_e}}{\left[ e^{2E/RT} + \left( \frac{f_2 k_o}{f_1 C} \right)^2 R_B \right]^{1/2}} \quad (5)$$

B-1

UNCLASSIFIED

UNCLASSIFIED

For the normalized mass loss rates a similar series of substitutions gave

$$\dot{m} \sqrt{\frac{R_B}{P_e}} = \frac{k_o e^{-E/RT}}{\left[ \frac{1}{R_B} + \left( \frac{k_o}{C} \right)^2 e^{-2E/RT} \right]^{1/2}} \quad (6)$$

for curves expressed in terms of the theory (Figures 35 and 54).

The theory curves modified to correspond to data points acquired in their actual environments were determined from

$$\dot{m}' \sqrt{\frac{R_B}{P_e}} = \frac{f_2 k_o e^{-E/RT}}{\left[ \frac{1}{R_B} + \left( \frac{f_2 k_o}{f_1 C} \right)^2 e^{-2E/RT} \right]^{1/2}} \quad (7)$$

This arrangement was used to relate the ATJ data more clearly with respect to the theory (Figure 34).

In order to correlate data points with the theory curves (as represented by eq'ns. (4) and (6), a slightly different approach was used in which it was necessary to determine a weighting factor for each test point. To establish this factor a tabulation of  $\dot{m}$  was made for conditions under which the ratio of  $\dot{m}_R / \dot{m}_D$  assumed particular values. For each material, the ratio

$$\frac{\dot{m}_R}{\dot{m}_D} = \frac{k_o \sqrt{R_B} e^{-E/RT}}{C}$$

was evaluated and the appropriate range of temperatures was determined for each size specimen. The extent to which each mass rate ( $\dot{m}_D, \dot{m}_R$ )

UNCLASSIFIED

contributed to the combined mass rate ( $\dot{m}$ ) for the corresponding condition was evaluated as the weighting factor for the datum point. See Appendix C.

For a given set of nominal operating conditions, the factors  $f_1$  and  $f_2$  were dependent upon the shock Reynolds number and hence were treated as constants to which the weighting factors were applied.

In the preceding equations:

	ATJ Graphite
$k_o$ (lb./sec.-ft <sup>2</sup> -atm <sup>1/2</sup> )	$4.42 \times 10^5$
E (cal/mole)	$44.0 \times 10^3$
C (lb./sec.-ft <sup>3/2</sup> -atm <sup>1/2</sup> )	$6.2 \times 10^{-3}$

## APPENDIX C

### DISCUSSION AND PRESENTATION OF SAMPLE CALCULATIONS REGARDING DATA REDUCTION

To illustrate the process of reducing mass rate data in the experimental program, the results of two test runs are presented and carried through each of the calculations used. Where necessary, details of the specific procedures are expanded.

Consider the results of runs 521 and 560 on 1/16" diameter ATJ graphite mass rate specimens (Table 15):

Run No.	Time sec.	Length Chg. inches	Mass Loss lb/ft. <sup>2</sup>	Mass Rate lb/sec.ft. <sup>2</sup>	Ave. Surf. Temp. °K
560	250	.0750	.6751	---	---
521	60	.0166	.1494	---	---
	190	.0584	.5257	$2.77 \times 10^{-3}$	1515

Difference in time and mass loss between the two runs at the same test conditions result in one mass rate data point at an average surface temperature ( $T_w$ ) of 1515°K.

$$\dot{m}' = \frac{\Delta m}{\Delta t} = \frac{\rho \Delta l}{12 \Delta t} = \frac{108 \times .0584}{12 \times \Delta t} = \frac{.5257}{\Delta t}$$

$$\dot{m}' = 2.77 \times 10^{-3} \text{ lb/sec.ft.}^2 \text{ (data pt. Figure 32, sym. } \bullet \text{)}$$

Other data, useful later in the computations are:

Reynolds number per foot =  $520 \text{ ft.}^{-1}$

Reynolds number,  $Re_s = 520 \times \frac{1}{16} \times \frac{1}{12} = 2.7$

Effective radius,  $R_B = 2.46 \times \frac{1}{32} \times \frac{1}{12} = 6.41 \times 10^{-3} \text{ ft.}$

Model stagnation pressure,  $P_e = 7.70 \times 10^{-3} \text{ atmos.}$

The individual data points ( $\dot{m}'$ ) were located on an Arrhenius plot ( $\dot{m}'$  vs  $1/T$ , Figure 32). Collectively, they were used to establish a reaction rate slope from which the specific reactivity ( $k_o$ ) and activation energy ( $E$ ) of the ATJ graphite were evaluated. The values obtained were expressed in a reaction rate equation, which when coupled with the theoretical expression for diffusion controlled activity by the transition equation, provided a single equation (Appendix B) from which "theoretical" performance curves were evaluated. These were overplotted on the Arrhenius graph (Figure 32).

The computed mass rates are for data acquired in regimes other than those of high Reynolds number, for which the original theory was derived. Hence experimental data have to be modified to correspond to the theory. The value of the modification factor ( $F_m$ ) depends on the degree to which oxidation is rate controlled or diffusion controlled. The plotted theory curves depict graphically a qualitative sense of the contribution of each process and indicate that the modifying factor required by either process must be weighted against that of the other process depending on their relative predominance for a given test point. The following discussion constitutes the basis for obtaining a "weight" applicable to a given data point. Every point was individually weighted.

$$\dot{m} = \left[ \frac{1}{\dot{m}_D^2} + \frac{1}{\dot{m}_R^2} \right]^{1/2} \quad (\text{Transition equation, Sec. II C, eq'n 30})$$

Let  $N = \dot{m}_R / \dot{m}_D$  ( $0 \leq N \leq \infty$ ). Then

$$\dot{m} = \left[ \frac{1}{\dot{m}_D^2} + \frac{1}{N^2 \dot{m}_D^2} \right]^{1/2} = \frac{\dot{m}_D}{\left[ 1 + \frac{1}{N^2} \right]^{1/2}}$$

Divide both sides by  $\dot{m}_D$

$$\frac{\dot{m}}{\dot{m}_D} = \frac{1}{\left[ 1 + \frac{1}{N^2} \right]^{1/2}} = \frac{N}{\left[ N^2 + 1 \right]^{1/2}}$$

The ratio gives  $0 \leq \frac{\dot{m}}{\dot{m}_D} \leq 1$ , which has the virtue of excluding explicit use of mass rates in the right hand member. For any given value of  $N$ , the contributing mass rates are  $\dot{m}_D$  and  $\dot{m}_R = N\dot{m}_D$ .

The relative contribution of either process can be seen in the expression:

$$\frac{\dot{m}}{\dot{m}_D} = \frac{1}{\left[ 1 + \frac{1}{N^2} \right]^{1/2}}$$

If  $\dot{m}_R$  is  $N$  times  $\dot{m}_D$  (as postulated), it contributes  $\frac{1}{N^2}$  toward the value of  $\dot{m}$  when  $\dot{m}_D$  contributes unity, relative to it. Their total contribution is  $1 + \frac{1}{N^2}$  and their fractional contributions are

$$\text{for } \dot{m}_R; \quad \frac{1/N^2}{1 + 1/N^2} = \frac{1}{1 + N^2}$$

$$\text{for } \dot{m}_D; \quad \frac{1}{1 + 1/N^2} = \frac{N^2}{1 + N^2}$$



Note that for  $N \rightarrow \infty$ , ratio  $\dot{m}/\dot{m}_D \rightarrow 1$ . (diff. control)

$N \rightarrow 0$ , ratio  $\dot{m}/\dot{m}_D \rightarrow N$  (rate control)

$N = 1$ , ratio  $\dot{m}/\dot{m}_D \rightarrow \frac{1}{2}\sqrt{2}$  (equal control)

Numerical solutions follow:

$$\frac{\dot{m}_R}{\dot{m}_D} = N = \frac{k_o \sqrt{P_e} e^{-E/RT}}{\sqrt{C \frac{P_e}{R_B}}} = \frac{k_o \sqrt{R_B} e^{-E/RT}}{C}$$

where  $C$  is the diffusion control level in  $\text{lb/ft.}^{3/2}\text{-sec-atm}^{1/2}$

$$\text{Then } N = \frac{4.42 \times 10^5 (e^{-22150/1515})}{6.2 \times 10^{-3} (384)^{1/2}}$$

$$N = \frac{7.15 \times 10^7}{19.6 (2.705 \times 10^6)}$$

$$N = 1.35$$

Thus, the contributed fractions are

$$\text{for } \dot{m}_R; \quad \frac{1}{1 + N^2} = .335$$

$$\text{for } \dot{m}_D; \quad \frac{N^2}{1 + N^2} = .645; \text{ where } .645 + .355 = 1.00$$

For the 1/16" diameter mass rate models,  $Re_s = 2.7$ ; using this value one obtains a Stanton Number ratio ( $f_1$ ) of 0.60 (Figure 22) for the diffusion controlled oxidation and an effective pressure ratio ( $f_2$ ) of 0.44 (Figure 23) for rate controlled oxidation.

Then

$$\frac{f_1 N^2}{1 + N^2} + \frac{f_2}{1 + N^2} = F_m; \text{ Weighted Modifying Factor}$$

$$0.60 (0.645) + 0.44(0.355) = 0.543$$

The originally calculated data point can now be modified,  $\dot{m}'/F_m = \dot{m}$ ,

$$\text{thus, } \dot{m} = \frac{2.77 \times 10^{-3}}{0.543} = 5.22 \times 10^{-3} \text{ lb/sec.ft.}^2 (\text{data pt., Figure 33})$$

giving the value of the mass rate corresponding to that predicted by the original theory. The value of  $\dot{m}'$  or of  $\dot{m}$  may be normalized with respect to body radius and pressure and plotted against surface temperature (for this pt.,  $T_w = 1515^\circ\text{K}$ ).

Therefore,

$$\begin{aligned} \dot{m}' \sqrt{\frac{R_B}{P_e}} &= 2.77 \times 10^{-3} \left( \frac{6.41 \times 10^{-3}}{7.70 \times 10^{-3}} \right)^{1/2} \\ &= 2.54 \times 10^{-3} \text{ lb/ft}^{3/2} \text{-sec-atm}^{1/2} (\text{data pt. Figure 34}) \end{aligned}$$

Similarly,

$$\begin{aligned} \dot{m} \sqrt{\frac{R_B}{P_e}} &= 5.22 \times 10^{-3} \left( \frac{6.41 \times 10^{-3}}{7.70 \times 10^{-3}} \right)^{1/2} \\ &= 4.78 \times 10^{-3} \text{ lb/ft}^{3/2} \text{-sec-atm}^{1/2} (\text{data pt. Figure 35}) \end{aligned}$$

Thus, each datum point for comparison with the theory is established, calculated in the form pertinent to the type presentation for which it is to be used.

UNCLASSIFIED

TABLE 1  
SUMMARY OF TOTAL CALORIMETER  
ENTHALPY MEASUREMENTS

$E_k, \text{KW}$	$\dot{m}, \text{lb/sec.}$	$P_s, \text{psia}$	$h_s/RT_o$	$h_s, \text{Btu/lb.}$
238	.0015	22.2	351	11690
238	↓	20.8	327	11070
230		20.6	316	10700
283	↓	19.5	332	11230
76.7	.0014	16.0	157	5310
76.7	↓	15.9	166	5610
76.7		16.0	162	5480
87.5	↓	16.3	162	5480

UNCLASSIFIED

UNCLASSIFIED

TABLE 2  
SUMMARY OF COLD WALL HEAT TRANSFER MEASUREMENTS  
FLAT FACE SPECIMENS

Configuration (1)	Nozzle	Position (2)	Nominal $h_g/RT_o$	Heat Transfer Rates
1"D-1/4"d	5.0"	0.563"	350	75.0 Btu/ft <sup>2</sup> -sec
		1.500		76.0
		"		68.5
		1.850		76.0
		"		63.5
		"		58.5
		2.225		71.5
		"		69.5
		0.563		144.5
		"		139.0
1/4"D-1/8"d		1.500		141.0
1/4"D-1/8"d (3)		0.563		130.0
1/4"D-1/8"d (3)	1.2	0.563		482
1/16"d (3)		"		497
		"		505
	5.0	1.500		269
		"		283
		"		288
1"D-1/4"d	5.0	0.800	160	49.0
		"		48.6

- (1) Configuration: Gives model dia. followed by copper insert dia.  
 (2) Station: Distance to stagnation point, from nozzle exit  
 (3) Copper cylinder with .003" RTV coating

UNCLASSIFIED

# UNCLASSIFIED

TABLE 3  
SUMMARY OF MASS RATE DATA

Specimen Dia.	1/4"	Notes -
Specimen Mat'l	ATJ	(1) Unmodified data
Nozzle Exit Dia.	5"	(2) Data modified for
Stag'n Press., atm	$8.25 \times 10^{-3}$	Reynolds No. Effects
Enthalpy Ratio	350	<input checked="" type="checkbox"/> Symbol on graphs
Reynolds No., $Re_s$	11	

Run Nos.	Time Sec.	Mass Loss Lb/ft. <sup>2</sup>	Avg. °K Temp.	Mass Rate $\times 10^3$ lb/ft <sup>2</sup> - sec		$m \sqrt{\frac{R_b}{P_e}} \times 10^3$ lb/ft <sup>3/2</sup> - sec - Atm <sup>1/2</sup>	
				(1)	(2)	(1)	(2)
472	80	.1197					
463	39	.0459					
	41	.0738	1425	1.93	2.185	3.42	3.875
473	120	.1980					
472	80	.1197					
	40	.0783	1465	1.995	2.065	3.53	3.83
462	127	.2187					
472	80	.1197					
	47	.0990	1480	2.155	2.35	3.56	3.88
474	160	.2898					
462	127	.2187					
	33	.0711	1405	2.195	2.52	3.57	4.13
474	160	.2898					
473	120	.1980					
	40	.0918	1435	2.34	2.64	3.60	4.06
473	120	.1980					
463	39	.0459					
	81	.1521	1400	1.915	2.225	3.39	3.93
458	128	.1791					
461	100	.1377					
	28	.0414	1385	1.54	1.82	2.72	3.21
458	128	.1791					
459	100	.1089					
	28	.0702	1370	2.56	3.06	4.53	5.42
474	160	.2898					
461	100	.1377					
	60	.1521	1410	2.585	2.965	4.58	5.26
474	160	.2898					
459	100	.1089					
	60	.1809	1400	3.075	3.57	5.44	6.30

UNCLASSIFIED

# UNCLASSIFIED

TABLE 3  
SUMMARY OF MASS RATE DATA

Specimen Dia.	1/4"	Notes -
Specimen Mat'l	ATJ	(1) Unmodified data
Nozzle Exit Dia.	5"	(2) Data modified for
Stag'n Press., atm	$8.25 \times 10^{-3}$	Reynolds No. Effects
Enthalpy Ratio	350	<input checked="" type="checkbox"/> Symbol on graphs
Reynolds No., $Re_s$	11	

Run Nos.	Time Sec.	Mass Loss Lb/ft. <sup>2</sup>	Avg. °K Temp.	Mass Rate $\times 10^3$ lb/ft <sup>2</sup> - sec		$\dot{m} \sqrt{\frac{Rb}{Pe}} \times 10^3$ lb/ft <sup>3/2</sup> - sec - Atm <sup>1/2</sup>	
				(1)	(2)	(1)	(2)
473	120	.1980					
461	100	.1377					
	20	.0603	1410	3.07	3.53	5.43	6.24
462	127	.2187					
461	100	.1377					
	27	.0810	1405	3.06	3.55	5.42	6.28
462	127	.2187					
473	120	.1980					
	7	.0207	1425	3.015	3.415	5.34	6.05
474	160	.2898					
472	80	.1197					
	80	.1701	1440	2.175	2.44	3.87	4.34
463	39	.0459	1300	1.20	1.655	2.12	2.92
461	100	.1377	1320	1.40	1.825	2.48	4.05
473	120	.1980	1300	1.68	2.035	2.97	3.61
462	127	.2187	1340	1.79	2.25	3.16	3.97
474	160	.2898	1300	1.85	2.25	3.28	3.99

# UNCLASSIFIED

UNCLASSIFIED

TABLE 4  
SUMMARY OF MASS RATE DATA

Specimen Dia. 1/4" Notes -  
 Specimen Mat'l ATJ (1) Unmodified data  
 Nozzle Exit Dia. 1.2" (2) Data modified for  
 Stag'n Press., atm  $5.60 \times 10^{-2}$  Reynolds No. Effects  
 Enthalpy Ratio 350  $\odot$  Symbol on graphs  
 Reynolds No.,  $Re_s$  85

Run Nos.	Time Sec.	Mass Loss Lb/ft. <sup>2</sup>	Avg. °K Temp.	Mass Rate $\times 10^3$ lb/ft <sup>2</sup> - sec		$\dot{m} \sqrt{\frac{Rb}{Pe}} \times 10^3$ lb/ft <sup>3/2</sup> - sec - Atm <sup>1/2</sup>	
				(1)	(2)	(1)	(2)
496	80	.8415					
494	45	.4392					
	35	.4023	2150	11.50	8.86	7.80	6.07
501	87.5	.9702					
494	45	.4392					
	42.5	.5310	2125	12.48	9.71	8.46	6.58
495	100	1.0404					
494	45	.4392					
	55	.6012	2175	11.14	8.68	7.56	5.88
489	100	1.0593					
494	45	.4392					
	55	.6201	2230	11.29	8.77	7.65	5.95
490	130	1.4103					
494	45	.4392					
	85	.9711	2660	11.42	8.84	7.75	6.00
498	130	1.4490					
494	45	.4392					
	85	1.0108	2160	11.83	9.19	8.02	6.24
497	160	1.7460					
494	45	.4392					
	115	1.3068	2160	11.34	8.81	7.69	5.98
488	165	1.9440					
494	45	.4392					
	120	1.4048	2320	11.70	9.08	7.94	6.16
501	100	1.0602					
494	45	.4392					
	55	.6210	2180	11.28	8.77	7.65	5.95

UNCLASSIFIED

# UNCLASSIFIED

TABLE 4  
SUMMARY OF MASS RATE DATA

Specimen Dia.	1/4"	Notes -
Specimen Mat'l	ATJ	(1) Unmodified data
Nozzle Exit Dia.	1.2"	(2) Data modified for
Stag'n Press., atm	$5.60 \times 10^{-2}$	Reynolds No. Effects
Enthalpy Ratio	350	⊙ Symbol on graphs
Reynolds No., $Re_s$	85	

Run Nos.	Time Sec.	Mass Loss Lb/ft. <sup>2</sup>	Avg. °K Temp.	Mass Rate $\times 10^3$ lb/ft <sup>2</sup> - sec		$\dot{m} \sqrt{\frac{Rb}{Pe}} \times 10^3$ lb/ft <sup>3/2</sup> - sec - Atm <sup>1/2</sup>	
				(1)	(2)	(1)	(2)
489	100	1.0593					
496	80	.8415					
	20	.2178	2230	11.88	9.24	8.05	6.25
501	100	1.0602					
496	80	.8415					
	20	.2187	2180	11.90	9.25	8.07	6.28
498	130	1.4490					
496	80	.8415					
	50	.6075	2160	12.14	9.44	8.23	6.39
490	130	1.4103					
496	80	.8415					
	50	.5688	2660	11.37	8.80	7.71	5.97
497	160	1.7460					
496	80	.8415					
	80	.9045	2160	11.30	8.79	7.66	5.95
488	165	1.9440					
496	80	.8415					
	85	1.1025	2320	12.95	10.08	8.78	6.72
498	130	1.4490					
501	87.5	.9702					
	42.5	.4788	2135	11.28	8.77	7.65	5.95
488	165	1.9440					
501	87.5	.9702					
	77.5	.9738	2290	12.57	9.76	8.52	6.62
490	130	1.4103					
495	100	1.0404					
	30	.3699	2685	12.32	9.55	8.35	6.45

# UNCLASSIFIED



TABLE 4  
SUMMARY OF MASS RATE DATA

Specimen Dia. 1/4" Notes -  
 Specimen Mat'l ATJ (1) Unmodified data  
 Nozzle Exit Dia. 1.2" (2) Data modified for  
 Stag'n Press., atm  $5.60 \times 10^{-2}$  Reynolds No. Effects  
 Enthalpy Ratio 350  $\odot$  Symbol on graphs  
 Reynolds No.,  $Re_s$  85

Run Nos.	Time Sec.	Mass Loss Lb/ft. <sup>2</sup>	Avg. °K Temp.	Mass Rate $\times 10^3$ lb/ft <sup>2</sup> - sec		$\dot{m} \sqrt{\frac{Rb}{Pe}} \times 10^3$ lb/ft <sup>3/2</sup> - sec - Atm <sup>1/2</sup>	
				(1)	(2)	(1)	(2)
497	160	1.7460					
495	100	1.0404					
	60	.7056	2185	11.77	9.14	7.98	6.20
488	165	1.9440	2350	11.77	9.11	7.98	6.11
498	130	1.4490	2170	11.13	8.66	7.55	5.87
501	87.5	.9702	2100	11.08	8.62	7.51	5.85
490	130	1.4103					
489	100	1.0593					
	30	.3510	2740	11.70	9.06	7.94	6.17
497	160	1.7640					
489	100	1.0593					
	60	.7047	2280	11.77	9.15	7.98	6.20
490	130	1.4103					
501	100	1.0602					
	30	.3501	2690	11.69	9.05	7.92	6.06
497	160	1.7640					
501	100	1.0602					
	60	.7038	2190	11.72	9.13	7.95	6.11
497	160	1.7640					
490	130	1.4103					
	30	.3537	2670	11.76	9.10	7.98	6.18

# UNCLASSIFIED

TABLE 5  
SUMMARY OF MASS RATE DATA

Specimen Dia.	1"	Notes -
Specimen Mat'l	ATJ	(1) Unmodified data
Nozzle Exit Dia.	5"	(2) Data modified for
Stag'n Press., atm	$9.7 \times 10^{-3}$	Reynolds No. Effects
Enthalpy Ratio	400	$\Delta$ Symbol on graphs
Reynolds No., $Re_s$	44	

Run Nos.	Time Sec.	Mass Loss Lb/ft. <sup>2</sup>	Avg. °K Temp.	Mass Rate $\times 10^3$ lb/ft <sup>2</sup> - sec		$\dot{m} \sqrt{\frac{Rb}{Pe}} \times 10^3$ lb/ft <sup>3/2</sup> - sec - Atm <sup>1/2</sup>	
				(1)	(2)	(1)	(2)
303	120	.0936					
305	60	.0324					
	60	.0612	1235	1.019	1.112	3.31	3.61
308	150	.1224					
305	60	.0324					
	90	.0900	1245	1.00	1.080	3.25	3.51
311	180	.1467					
305	60	.0324					
	120	.1143	1245	.939	1.013	3.05	3.19
316	240	.2007					
305	60	.0324					
	180	.1683	1245	.897	.969	2.92	3.15
307	110	.0828					
306	100	.0711					
	10	.0117	1280	1.171	1.211	3.81	3.94
303	120	.0936					
306	100	.0711					
	20	.0225	1290	1.127	1.139	3.68	3.72
308	150	.1224					
306	100	.0711					
	50	.0513	1300	1.023	1.021	3.33	3.32
311	180	.1467					
306	100	.0711					
	80	.0756	1300	.947	.945	3.08	3.07
316	240	.2007					
306	100	.0711					
	140	.1296	1300	.926	.925	3.01	3.00
303	120	.0936					
307	110	.0828					
	10	.0108	1300	1.082	1.080	3.52	3.51

UNCLASSIFIED

UNCLASSIFIED

TABLE 5  
SUMMARY OF MASS RATE DATA

Specimen Dia.	1"	Notes -
Specimen Mat'l	ATJ	(1) Unmodified data
Nozzle Exit Dia.	5"	(2) Data modified for
Stag'n Press., atm	$9.7 \times 10^{-3}$	Reynolds No. Effects
Enthalpy Ratio	400	$\Delta$ Symbol on graphs
Reynolds No., $Re_s$	44	

Run Nos.	Time Sec.	Mass Loss Lb/ft. <sup>2</sup>	Avg. °K Temp.	Mass Rate $\times 10^3$ lb/ft <sup>2</sup> - sec		$\dot{m} \sqrt{\frac{Rb}{Pe}} \times 10^3$ lb/ft <sup>3/2</sup> - sec - Atm <sup>1/2</sup>	
				(1)	(2)	(1)	(2)
308	150	.1224					
307	110	.0828					
	40	.0396	1310	.988	.968	3.21	3.16
311	180	.1467					
307	110	.0828					
	70	.0639	1310	.909	.892	2.96	2.91
316	240	.2007					
307	110	.0828					
	130	.1179	1310	.906	.890	2.94	2.89
308	150	.1224					
303	120	.0936					
	30	.0288	1320	.964	.930	3.13	3.02
311	180	.1467					
303	120	.0936					
	60	.0531	1320	.885	.854	2.88	2.78
316	240	.2007					
303	120	.0936					
	120	.1071	1320	.890	.859	2.90	2.80
311	180	.1467					
308	150	.1224					
	30	.0243	1330	.811	.770	2.64	2.505
316	240	.2007					
308	150	.1224					
	90	.0783	1330	.868	.823	2.82	2.68
316	240	.2007					
311	180	.1467					
	60	.0540	1330	.902	.856	2.93	2.78

UNCLASSIFIED

UNCLASSIFIED

TABLE 5  
SUMMARY OF MASS RATE DATA

Specimen Dia.	1"	Notes -
Specimen Mat'l	ATJ	(1) Unmodified data
Nozzle Exit Dia.	5"	(2) Data modified for
Stag'n Press., atm	$9.7 \times 10^{-3}$	Reynolds No. Effects
Enthalpy Ratio	400	$\Delta$ Symbol on graphs
Reynolds No., $Re_s$	44	

Run Nos.	Time Sec.	Mass Loss Lb/ft. <sup>2</sup>	Avg. °K Temp.	Mass Rate $\times 10^3$ lb/ft <sup>2</sup> - sec		$\dot{m} \sqrt{\frac{Rb}{Pe}} \times 10^3$ lb/ft <sup>3/2</sup> - sec - Atm <sup>1/2</sup>	
				(1)	(2)	(1)	(2)
327	300	.720					
323	63	.126					
	237	.594	1670	2.50	2.075	8.12	6.23
326	240	.567					
323	63	.126					
	177	.441	1685	2.49	2.065	8.10	6.21
322	213	.495					
323	63	.126					
	150	.369	1745	2.46	2.03	8.00	6.10
325	139	.297					
323	63	.126					
	76	.171	1685	2.31	1.908	7.52	5.74
327	300	.720					
324	77	.153					
	223	.567	1680	2.54	2.108	8.25	6.32
326	240	.567					
324	77	.153					
	163	.414	1695	2.54	2.108	8.25	6.32
322	213	.495					
324	77	.153					
	136	.342	1755	2.52	2.075	8.19	6.24
325	139	.297					
324	77	.153					
	62	.144	1695	2.33	1.934	7.58	5.82
327	300	.720					
325	139	.297					
	161	.423	1690	2.63	2.18	8.55	6.55

UNCLASSIFIED

# UNCLASSIFIED

TABLE 5  
SUMMARY OF MASS RATE DATA

Specimen Dia.	1"	Notes -
Specimen Mat'l	ATJ	(1) Unmodified data
Nozzle Exit Dia.	5"	(2) Data modified for
Stag'n Press., atm	$9.7 \times 10^{-3}$	Reynolds No. Effects
Enthalpy Ratio	400	$\Delta$ Symbol on graphs
Reynolds No., $Re_s$	44	

Run Nos.	Time Sec.	Mass Loss Lb/ft. <sup>2</sup>	Avg. °K Temp.	Mass Rate $\times 10^3$ lb/ft <sup>2</sup> - sec		$\dot{m} \sqrt{\frac{Rb}{Pe}} \times 10^3$ lb/ft <sup>3/2</sup> - sec - Atm <sup>1/2</sup>	
				(1)	(2)	(1)	(2)
326	240	.567					
325	139	.297					
	101	.270	1710	2.67	2.21	8.68	6.63
322	213	.495					
325	139	.297					
	74	.198	1770	2.68	2.21	8.71	6.64
327	300	.720					
322	213	.495					
	87	.225	1750	2.59	2.138	8.42	6.43
326	240	.567					
322	213	.495					
	27	.072	1770	2.67	2.20	8.68	6.61
327	300	.720					
326	240	.567					
	60	.153	1690	2.55	2.115	8.29	6.35
323	63	.126	1350	2.00	1.833	6.50	6.02
324	77	.153	1450	1.99	1.73	6.47	5.63
325	139	.297	1450	2.14	1.86	6.95	6.04
322	213	.495	1750	2.32	1.915	7.54	5.75
326	240	.567	1630	2.37	1.975	7.70	5.93
327	300	.720	1600	2.40	2.008	7.80	6.03

# UNCLASSIFIED

UNCLASSIFIED

TABLE 6  
SUMMARY OF MASS RATE DATA

Specimen Dia.	1"	Notes -
Specimen Mat'l	ATJ	(1) Unmodified data
Nozzle Exit Dia.	1.2"	(2) Data modified for
Stag'n Press., atm	$4.43 \times 10^{-2}$	Reynolds No. Effects
Enthalpy Ratio	400	◇ Symbol on graphs
Reynolds No., $Re_s$	342	

Run Nos.	Time Sec.	Mass Loss Lb/ft.	Avg. °K Temp.	Mass Rate $\times 10^3$ lb/ft <sup>2</sup> - sec		$\dot{m} \sqrt{\frac{R_b}{P_e}} \times 10^3$ lb/ft <sup>3/2</sup> - sec - Atm <sup>1/2</sup>	
				(1)	(2)	(1)	(2)
342	200	1.0017					
330	39	.216					
	161	0.7857	2050	4.88	3.71	7.46	5.68
331	100	.513					
330	39	.216					
	61	.297	1825	4.88	3.74	7.46	5.73
342	200	1.0017					
336	60	.2970					
	140	.7047	1790	5.05	3.88	7.71	5.92
331	100	.513					
336	60	.297					
	40	.216	1960	5.39	4.10	8.24	6.28
342	200	1.0017					
331	100	.513					
	100	.4887	2115	4.86	3.69	7.42	5.65
342	200	1.0017					
332	150	.729					
	50	.2727	2135	5.45	4.14	8.33	6.30
342	200	1.0017	1600	5.01	3.93	7.66	6.00
331	100	.513	2050	5.12	3.89	7.83	5.95
330	39	.216	1600	5.53	4.32	8.45	6.13

UNCLASSIFIED

UNCLASSIFIED

TABLE 7  
SUMMARY OF MASS RATE DATA

Specimen Dia. 1/16" Notes -  
 Specimen Mat'l ATJ (1) Unmodified data  
 Nozzle Exit Dia. 5" (2) Data modified for  
 Stag'n Press., atm  $7.70 \times 10^{-3}$  Reynolds No. Effects  
 Enthalpy Ratio 350  
 Reynolds No.,  $Re_s$  2.7  $\odot$  Symbol on graphs

Run Nos.	Time Sec.	Mass Loss Lb/ft. <sup>2</sup>	Avg. °K Temp.	Mass Rate $\times 10^3$ lb/ft <sup>2</sup> - sec		$\dot{m} \sqrt{\frac{Rb}{Pe}} \times 10^3$ lb/ft <sup>3/2</sup> - sec - Atm <sup>1/2</sup>	
				(1)	(2)	(1)	(2)
560	250	.6751					
521	60	.1494					
	190	.5257	1515	2.77	5.21	2.54	4.78
560	250	.6751					
520	120	.3168					
	130	.3583	1520	2.75	5.15	2.52	4.73
560	250	.6751					
519	120	.2988					
	130	.3763	1540	2.90	5.38	2.66	4.94
560	250	.6751					
518	100	.2556					
	150	.4195	1545	2.80	5.17	2.56	4.73
560	250	.6751					
517	100	.2520					
	150	.4231	1560	2.82	5.15	2.58	4.72
560	250	.6751					
516	80	.1863					
	170	.4888	1545	2.87	5.30	2.62	4.84
560	250	.6751					
515	80	.2007					
	170	.4744	1520	2.79	5.23	2.55	4.79
560	250	.6751					
514	60	.1620					
	190	.5131	1500	2.70	5.13	2.47	4.70
560	250	.6751					
513	40	.1107					
	210	.5644	1485	2.69	5.17	2.46	4.72

UNCLASSIFIED

UNCLASSIFIED

TABLE 7  
SUMMARY OF MASS RATE DATA

Specimen Dia. 1/16" Notes -  
 Specimen Mat'l ATJ (1) Unmodified data  
 Nozzle Exit Dia. 5" (2) Data modified for  
 Stag'n Press., atm  $7.70 \times 10^{-3}$  Reynolds No. Effects  
 Enthalpy Ratio 350 • Symbol on graphs  
 Reynolds No.,  $Re_s$  2.7

Run Nos.	Time Sec.	Mass Loss Lb/ft.. <sup>2</sup>	Avg. °K Temp.	Mass Rate $\times 10^3$ lb/ft <sup>2</sup> - sec		$\dot{m} \sqrt{\frac{Rb}{Pe}} \times 10^3$ lb/ft <sup>3/2</sup> - sec - Atm <sup>1/2</sup>	
				(1)	(2)	(1)	(2)
558	200	.5454					
557	100	.2205					
	100	.3249	1615	2.35	5.75	2.97	4.79
558	200	.5454					
521	60	.1494					
	140	.3960	1525	2.83	5.29	2.59	4.85
558	200	.5454					
520	120	.3168					
	80	.2286	1530	2.86	5.33	2.62	4.89
558	200	.5454					
519	120	.2988					
	80	.2466	1550	3.08	5.65	2.82	4.99
558	200	.5454					
518	100	.2556					
	100	.2898	1555	2.90	5.31	2.65	4.85
558	200	.5454					
517	100	.2520					
	100	.2934	1570	2.93	5.31	2.68	4.86
558	200	.5454					
516	80	.1863					
	120	.3591	1555	2.99	5.47	2.74	5.02
558	200	.5454					
515	80	.2007					
	120	.3447	1530	2.87	5.34	2.63	4.90
558	200	.5454					
514	60	.1620					
	140	.3834	1510	2.74	5.17	2.51	4.74

UNCLASSIFIED



# UNCLASSIFIED

TABLE 7  
SUMMARY OF MASS RATE DATA

Specimen Dia. 1/16" Notes -  
Specimen Mat'l ATJ (1) Unmodified data  
Nozzle Exit Dia. 5" (2) Data modified for  
Stag'n Press., atm  $7.70 \times 10^{-3}$  Reynolds No. Effects  
Enthalpy Ratio 350 • Symbol on graphs  
Reynolds No.,  $Re_s$  2.7

Run Nos.	Time Sec.	Mass Loss Lb/ft. <sup>2</sup>	Avg. °K Temp.	Mass Rate $\times 10^3$ lb/ft <sup>2</sup> - sec		$\dot{m} \sqrt{\frac{Rb}{Pe}} \times 10^3$ lb/ft <sup>3/2</sup> - sec - Atm <sup>1/2</sup>	
				(1)	(2)	(1)	(2)
558	200	.5454					
513	40	.1107					
	160	.4347	1495	2.72	5.20	2.49	4.75
559	150	.3954					
557	100	.2205					
	50	.1749	1640	3.49	6.22	3.19	5.69
559	150	.3954					
521	60	.1494					
	90	.2460	1550	2.73	5.02	2.50	4.60
559	150	.3954					
520	120	.3168					
	30	.0786	1555	2.62	4.79	2.40	4.40
559	150	.3954					
519	120	.2988					
	30	.0966	1575	3.22	5.85	2.95	5.35
559	150	.3954					
518	100	.2556					
	50	.1398	1580	2.79	5.05	2.55	4.62
559	150	.3954					
517	100	.2520					
	50	.1434	1595	2.87	5.15	2.63	4.72
559	150	.3954					
516	80	.1863					
	70	.2091	1580	2.98	5.40	2.72	4.92
559	150	.3954					
515	80	.2007					
	70	.1947	1555	2.78	5.09	2.54	4.65
559	150	.3754					
514	60	.1620					
	90	.2334	1535	2.54	4.65	2.32	4.25

UNCLASSIFIED

UNCLASSIFIED

TABLE 7  
SUMMARY OF MASS RATE DATA

Specimen Dia. 1/16" Notes -  
Specimen Mat'l ATJ (1) Unmodified data  
Nozzle Exit Dia. 5" (2) Data modified for  
Stag'n Press., atm  $7.70 \times 10^{-3}$  Reynolds No. Effects  
Enthalpy Ratio 350 \* Symbol on graphs  
Reynolds No.,  $Re_s$  2.7

Run Nos.	Time Sec.	Mass Loss Lb/ft. <sup>2</sup>	Avg. °K Temp.	Mass Rate $\times 10^3$ lb/ft <sup>2</sup> - sec		$\dot{m} \sqrt{\frac{Rb}{Pe}} \times 10^3$ lb/ft <sup>3/2</sup> - sec - Atm <sup>1/2</sup>	
				(1)	(2)	(1)	(2)
559	150	.3954					
513	40	.1107					
	110	.2847	1520	2.59	4.85	2.37	4.44
557	100	.2205					
513	40	.1107					
	60	.1098	1480	1.83	3.53	1.68	3.24
521	60	.1495					
513	40	.1107					
	20	.0588	1445	2.99	5.90	2.74	5.41
520	120	.3168					
521	60	.1494					
	60	.1674	1465	2.78	5.43	2.54	4.95
520	120	.3168					
518	100	.2556					
	20	.0612	1495	3.06	5.83	2.80	5.33
520	120	.3168					
517	100	.2520					
	20	.0648	1510	3.24	6.12	2.96	5.59
520	120	.3168					
516	80	.1863					
	40	.1305	1495	3.26	6.22	2.98	5.69
520	120	.3168					
515	80	.2007					
	40	.1161	1470	2.91	5.65	2.66	5.17
520	120	.3168					
514	60	.1620					
	60	.1548	1450	2.58	5.08	2.36	4.65

UNCLASSIFIED

UNCLASSIFIED

TABLE 7  
SUMMARY OF MASS RATE DATA

Specimen Dia. 1/16"  
Specimen Mat'l ATJ  
Nozzle Exit Dia. 5"  
Stag'n Press., atm  $7.70 \times 10^{-3}$   
Enthalpy Ratio 350  
Reynolds No.,  $Re_s$  2.7

Notes -  
(1) Unmodified data  
(2) Data modified for Reynolds No. Effects  
⊙ Symbol on graphs

Run Nos.	Time Sec.	Mass Loss Lb/ft. <sup>2</sup>	Avg. °K Temp.	Mass Rate $\times 10^3$ lb/ft <sup>2</sup> - sec		$\dot{m} \sqrt{\frac{Rb}{Pe}} \times 10^3$ lb/ft <sup>3/2</sup> - sec - Atm <sup>1/2</sup>	
				(1)	(2)	(1)	(2)
520	120	.3168					
513	40	.1107					
	80	.2061	1435	2.57	5.11	2.35	4.64
519	120	.2988					
521	60	.1494					
	60	.1494	1480	2.49	4.80	2.28	4.40
519	120	.2988					
518	100	.2556					
	20	.0432	1510	2.15	4.00	1.97	3.67
519	120	.2988					
517	100	.2520					
	20	.0468	1475	2.34	4.54	2.14	4.15
519	120	.2988					
516	80	.1863					
	40	.1125	1510	2.81	5.23	2.57	4.79
519	120	.2988					
515	80	.2007					
	40	.0979	1485	2.45	4.70	2.24	4.30
519	120	.2988					
514	60	.1620					
	60	.1368	1465	2.28	4.45	2.08	4.06
519	120	.2988					
513	40	.1107					
	80	.1881	1450	2.35	4.61	2.15	4.22
518	100	.2556					
521	60	.1494					
	40	.1062	1475	2.66	5.15	2.43	4.70

UNCLASSIFIED

# UNCLASSIFIED

TABLE 7  
SUMMARY OF MASS RATE DATA

Specimen Dia.	1/16"	Notes -
Specimen Mat'l	ATJ	(1) Unmodified data
Nozzle Exit Dia.	5"	(2) Data modified for
Stag'n Press., atm	$7.70 \times 10^{-3}$	Reynolds No. Effects
Enthalpy Ratio	350	● Symbol on graphs
Reynolds No., $Re_s$	2.7	

Run Nos.	Time Sec.	Mass Loss Lb/ft. <sup>2</sup>	Avg. °K Temp.	Mass Rate $\times 10^3$ lb/ft <sup>2</sup> - sec		$\dot{m} \sqrt{\frac{Rb}{Pe}} \times 10^3$ lb/ft <sup>3/2</sup> - sec - Atm <sup>1/2</sup>	
				(1)	(2)	(1)	(2)
518	100	.2556					
516	80	.1863					
	20	.0693	1505	3.46	6.55	3.16	5.99
518	100	.2556					
515	80	.2007					
	20	.0549	1480	2.74	5.20	2.51	4.84
518	100	.2556					
514	60	.1620					
	40	.0936	1460	2.34	4.58	2.14	4.17
518	100	.2556					
513	40	.1107					
	60	.1449	1445	2.41	4.75	2.21	4.36
517	100	.2520					
521	60	.1494					
	40	.1026	1495	2.56	4.89	2.34	4.47
517	100	.2520					
516	80	.1494					
	20	.0657	1525	3.29	6.15	3.01	5.63
517	100	.2520					
515	80	.2007					
	20	.0513	1500	2.56	4.85	2.34	4.45
517	100	.2520					
514	60	.1620					
	40	.0900	1480	2.24	4.26	2.05	3.95
517	100	.2520					
513	40	.1107					
	60	.1413	1465	2.35	4.59	2.15	4.19

# UNCLASSIFIED

# UNCLASSIFIED

TABLE 7  
SUMMARY OF MASS RATE DATA

Specimen Dia.	1/16"	Notes -
Specimen Mat'l	ATJ	(1) Unmodified data
Nozzle Exit Dia.	5"	(2) Data modified for
Stag'n Press., atm	$7.70 \times 10^{-3}$	Reynolds No. Effects
Enthalpy Ratio	350	● Symbol on graphs
Reynolds No., $Re_s$	2:7	

Run Nos.	Time Sec.	Mass Loss Lb/ft. <sup>2</sup>	Avg. °K Temp.	Mass Rate $\times 10^3$ lb/ft <sup>2</sup> - sec		$\dot{m} \sqrt{\frac{R_b}{P_e}} \times 10^3$ lb/ft <sup>3/2</sup> - sec - Atm <sup>1/2</sup>	
				(1)	(2)	(1)	(2)
516	80	.1863					
521	60	.1494					
	20	.0369	1470	1.85	3.60	1.69	3.28
516	80	.1863					
513	40	.1107					
	40	.0756	1440	1.89	3.74	1.73	3.43
515	80	.2007					
521	60	.1494					
	20	.0513	1475	2.56	5.00	2.34	4.53
515	80	.2007					
514	60	.1620					
	20	.0387	1460	1.93	3.77	1.77	3.46
515	80	.2007					
513	40	.1107					
	40	.0900	1445	2.24	4.42	2.05	4.04
521	60	.1494					
513	40	.1107					
	20	.0387	1445	1.94	3.82	1.78	3.51
514	60	.1620					
513	40	.1107					
	20	.0513	1445	2.56	5.05	2.34	4.62
521	60	.1494	1400	2.49	5.09	2.28	4.65
516	80	.1863	1460	2.33	4.55	2.13	4.17
520	120	.3168	1410	2.64	5.35	2.42	4.90

# UNCLASSIFIED

# UNCLASSIFIED

TABLE 8  
SUMMARY OF MASS RATE DATA

Specimen Dia.	1"	Notes -
Specimen Mat'l	ATJ	(1) Unmodified data
Nozzle Exit Dia.	5"	(2) Data modified for
Stag'n Press., atm	$7.00 \times 10^{-3}$	Reynolds No. Effects
Enthalpy Ratio	160	▽ Symbol on graphs
Reynolds No., $Re_s$	51	

Run Nos.	Time Sec.	Mass Loss Lb/ft. <sup>2</sup>	Avg. °K Temp.	Mass Rate $\times 10^3$ lb/ft <sup>2</sup> - sec		$m \sqrt{\frac{Rb}{Pe}} \times 10^3$ lb/ft <sup>3/2</sup> - sec - Atm <sup>1/2</sup>	
				(1)	(2)	(1)	(2)
631	1200	1.2195	1280	1.02	1.042	3.90	3.98
631	1200	1.2195					
634	240	.2232					
	960	.9963	1270	1.04	1.09	3.975	4.165
631	1200	1.2195					
642	310	.2305					
	890	.9890	1280	1.11	1.134	4.24	4.34
631	1200	1.2195					
635	360	.2979					
	840	.9216	1285	1.10	1.123	4.21	4.29
631	1200	1.2195					
633	463	.4626					
	737	.7569	1260	1.03	1.090	3.94	4.165
631	1200	1.2195					
639	600	.4707					
	600	.7488	1285	1.25	1.278	4.77	4.89
631	1200	1.2195					
638	720	.6138					
	480	.6057	1275	1.26	1.307	4.82	5.00
631	1200	1.2195					
643	772	.6462					
	428	.5733	1300	1.34	1.348	5.12	5.15
631	1200	1.2195					
644	801	.7137					
	399	.5058	1295	1.265	1.287	4.84	4.92
632	960	.6930	1260	0.722	.765	2.76	2.92

# UNCLASSIFIED

UNCLASSIFIED

TABLE 8  
SUMMARY OF MASS RATE DATA

Specimen Dia. 1" Notes -  
 Specimen Mat'l ATJ (1) Unmodified data  
 Nozzle Exit Dia. 5" (2) Data modified for  
 Stag'n Press., atm  $7.00 \times 10^{-3}$  Reynolds No. Effects  
 Enthalpy Ratio 160  $\nabla$  Symbol on graphs  
 Reynolds No.,  $Re_s$  51

Run Nos.	Time Sec.	Mass Loss Lb/ft. <sup>2</sup>	Avg. °K Temp.	Mass Rate $\times 10^3$ lb/ft <sup>2</sup> - sec		$\dot{m} \sqrt{\frac{Rb}{Pe}} \times 10^3$ lb/ft <sup>3/2</sup> - sec - Atm <sup>1/2</sup>	
				(1)	(2)	(1)	(2)
632	960	.6930					
634	240	.2232					
	720	.4698	1255	0.653	.695	2.66	3.045
632	960	.6930					
642	310	.2305					
	650	.4625	1260	0.713	.765	2.725	2.925
632	960	.6930					
635	360	.2979					
	600	.3951	1270	0.658	.690	2.515	2.64
632	960	.6930					
633	463	.4626					
	497	.2304	1245	0.464	.481	1.773	1.84
632	960	.6930					
641	480	.4104					
	480	.2826	1275	0.589	.610	2.25	2.33
632	960	.6930					
639	600	.4707					
	360	.2223	1270	0.618	.648	2.36	2.48
632	960	.6930					
638	720	.6138					
	240	.0792	1260	0.330	.350	1.262	1.339
632	960	.6930					
643	772	.6462					
	188	.0468	1210	0.249	.278	.947	1.062
644	801	.7137	1265	0.890	.938	3.405	3.585
644	801	.7137					
634	240	.2232					
	561	.4905	1325	0.885	.860	3.38	3.285

UNCLASSIFIED

# UNCLASSIFIED

TABLE 8  
SUMMARY OF MASS RATE DATA

Specimen Dia.	1"	Notes -
Specimen Mat'l	ATJ	(1) Unmodified data
Nozzle Exit Dia.	5"	(2) Data modified for
Stag'n Press., atm	$7.00 \times 10^{-3}$	Reynolds No. Effects
Enthalpy Ratio	160	▽ Symbol on graphs
Reynolds No., $Re_s$	51	

Run Nos.	Time Sec.	Mass Loss Lb/ft. <sup>2</sup>	Avg. °K Temp.	Mass Rate $\times 10^3$ lb/ft <sup>2</sup> - sec		$\dot{m} \sqrt{\frac{Rb}{Pe}} \times 10^3$ lb/ft <sup>3/2</sup> - sec - Atm <sup>1/2</sup>	
				(1)	(2)	(1)	(2)
644	801	.7137					
642	310	.2305					
	491	.4832	1255	0.985	1.048	3.76	4.00
644	801	.7137					
635	360	.2979					
	441	.4158	1340	0.944	.895	3.61	3.42
644	801	.7137					
633	463	.4626					
	338	.2511	1315	0.744	.733	2.85	2.91
644	801	.7137					
641	480	.4104					
	321	.3033	1270	0.942	.988	3.60	3.775
644	801	.7137					
639	600	.4707					
	201	.2430	1340	1.210	1.147	4.62	4.38
644	801	.7137					
638	720	.6138					
	81	.0999	1330	1.233	1.193	4.71	4.56
643	772	.6462					
634	240	.2232					
	532	.4230	1280	.795	.820	3.04	3.135
643	772	.6462					
642	310	.2305					
	462	.4157	1285	.900	.919	3.44	3.51
643	772	.6462					
635	360	.2979					
	412	.3483	1295	.845	.854	3.23	3.265

# UNCLASSIFIED



UNCLASSIFIED

TABLE 8  
SUMMARY OF MASS RATE DATA

Specimen Dia.	1"	Notes -
Specimen Mat'l	ATJ	(1) Unmodified data
Nozzle Exit Dia.	5"	(2) Data modified for
Stag'n Press., atm	$7.00 \times 10^{-3}$	Reynolds No. Effects
Enthalpy Ratio	160	▽ Symbol on graphs
Reynolds No., $Re_s$	51	

Run Nos.	Time Sec.	Mass Loss Lb/ft. <sup>2</sup>	Avg. °K Temp.	Mass Rate $\times 10^3$ lb/ft <sup>2</sup> - sec		$\dot{m} \sqrt{\frac{Rb}{Pe}} \times 10^3$ lb/ft <sup>3/2</sup> - sec - Atm <sup>1/2</sup>	
				(1)	(2)	(1)	(2)
643	772	.6462					
633	463	.4626					
	309	.1836	1270	.593	.622	2.265	2.38
643	772	.6462					
641	480	.4104					
	292	.2358	1225	.807	.893	3.085	3.42
643	772	.6462					
639	600	.4707					
	172	.1755	1295	1.021	1.031	3.90	3.94
643	772	.6462					
638	720	.6138					
	52	.0324	1285	0.623	.637	2.38	2.44
638	720	.6138	1225	0.853	.943	3.26	3.60
638	720	.6138					
634	240	.2232					
	480	.3906	1285	0.815	.832	3.12	3.18
638	720	.6138					
642	310	.2305					
	410	.3833	1290	0.935	.949	3.575	3.63
638	720	.6138					
635	360	.2979					
	360	.3159	1300	0.878	.883	3.36	3.38
638	720	.6138					
633	463	.4626					
	257	.1512	1275	0.588	.609	2.25	2.325
638	720	.6138					
641	480	.4104					
	240	.1034	1230	0.432	.494	1.65	1.89

UNCLASSIFIED

# UNCLASSIFIED

TABLE 8  
SUMMARY OF MASS RATE DATA

Specimen Dia.	1"	Notes -
Specimen Mat'l	ATJ	(1) Unmodified data
Nozzle Exit Dia.	5"	(2) Data modified for
Stag'n Press., atm	$7.00 \times 10^{-3}$	Reynolds No. Effects
Enthalpy Ratio	160	▽ Symbol on graphs
Reynolds No., $Re_s$	51	

Run Nos.	Time Sec.	Mass Loss Lb/ft. <sup>2</sup>	Avg. °K Temp.	Mass Rate $\times 10^3$ lb/ft <sup>2</sup> - sec		$\dot{m} \sqrt{\frac{Rb}{Pe}} \times 10^3$ lb/ft <sup>3/2</sup> - sec - Atm <sup>1/2</sup>	
				(1)	(2)	(1)	(2)
638	720	.6138					
639	600	.4707					
	120	.1431	1300	1.190	1.197	4.55	4.57
642	310	.2305	1250	0.745	.798	2.85	3.05
639	600	.4707	1245	0.785	.849	3.00	3.24
639	600	.4707					
634	240	.2232					
	360	.2475	1295	0.688	.695	2.63	2.66
639	600	.4707					
642	310	.2305					
	290	.2402	1225	0.829	.917	3.17	3.51
639	600	.4707					
635	360	.2979					
	240	.1728	1320	0.720	.703	2.75	2.69
639	600	.4707					
641	480	.4104					
	120	.0603	1240	0.504	.549	1.927	2.10
641	480	.4104	1255	0.855	.911	3.27	3.48
641	480	.4104					
634	240	.2232					
	240	.1872	1270	0.780	.817	2.98	3.125
641	480	.4104					
642	310	.2305					
	170	.1799	1275	1.068	1.108	4.08	4.23
641	480	.4104					
635	360	.2979					
	120	.1125	1285	0.938	.958	3.585	3.66

# UNCLASSIFIED

UNCLASSIFIED

TABLE 8  
SUMMARY OF MASS RATE DATA

Specimen Dia.	1"	Notes -
Specimen Mat'l	ATJ	(1) Unmodified data
Nozzle Exit Dia.	5"	(2) Data modified for
Stag'n Press., atm	$7.00 \times 10^{-3}$	Reynolds No. Effects
Enthalpy Ratio	160	▽ Symbol on graphs
Reynolds No., $Re_s$	51	

Run Nos.	Time Sec.	Mass Loss Lb/ft. <sup>2</sup>	Avg. °K Temp.	Mass Rate $\times 10^3$ lb/ft <sup>2</sup> - sec		$\dot{m} \sqrt{\frac{Rb}{Pe}} \times 10^3$ lb/ft <sup>3/2</sup> - sec - Atm <sup>1/2</sup>	
				(1)	(2)	(1)	(2)
635	360	.2979	1245	0.829	.899	3.17	3.44
635	360	.2979					
642	240	.2232					
	120	.0747	1290	0.623	.569	2.38	2.175
635	360	.2979					
634	310	.2305					
	50	.0674	1285	1.347	1.374	5.14	5.25

UNCLASSIFIED

UNCLASSIFIED

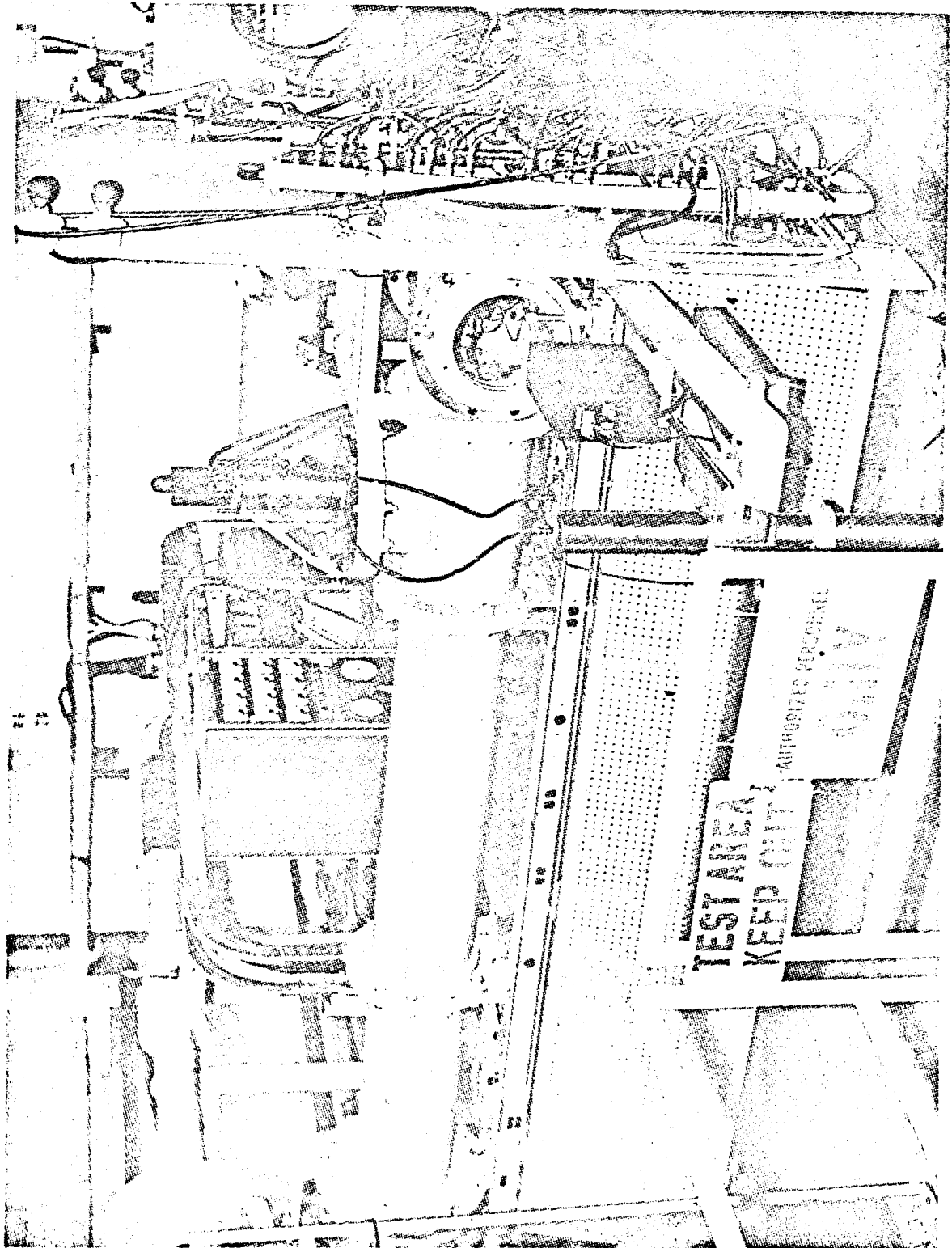


FIGURE 1 HYPERSOIC ARC HEATED WIND TUNNEL

UNCLASSIFIED

UNCLASSIFIED

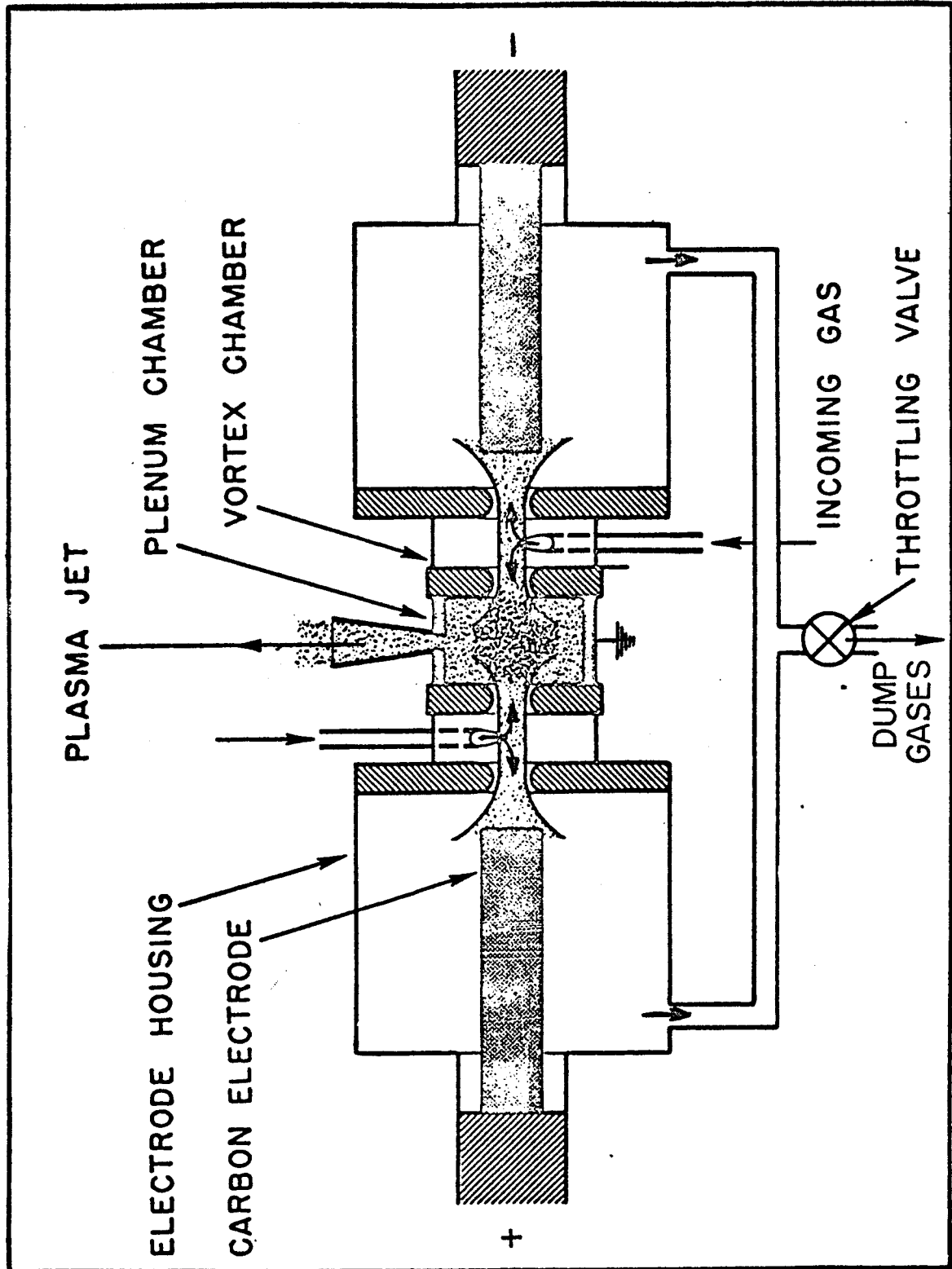


FIGURE 2 GENERAL ARRANGEMENT OF THE TANDEM GERDIEN PLASMA JET APPARATUS FOR ARC TUNNEL

UNCLASSIFIED

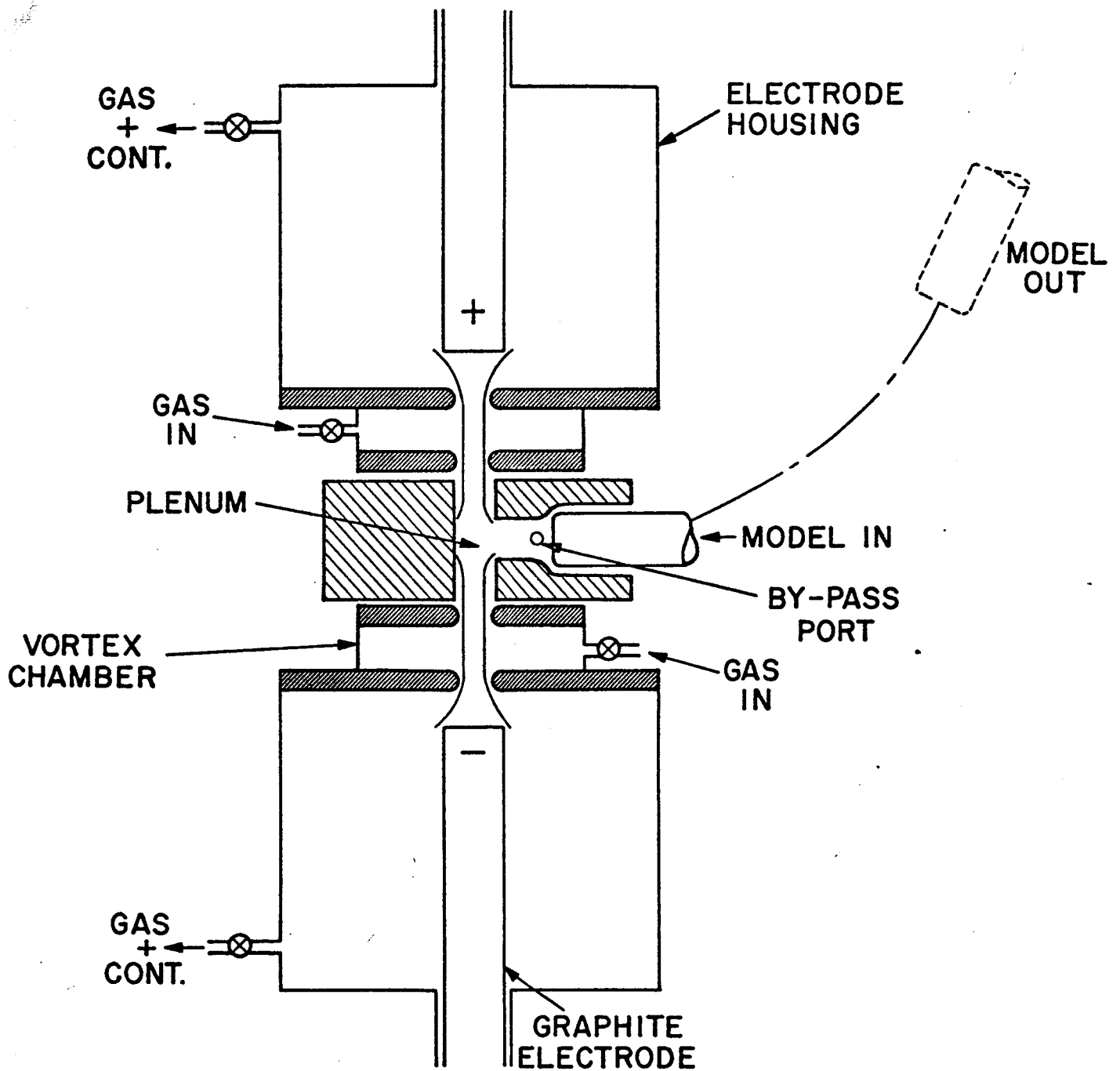


Figure 3a . GENERAL ARRANGEMENT TANDEM GERDIEN FREE JET

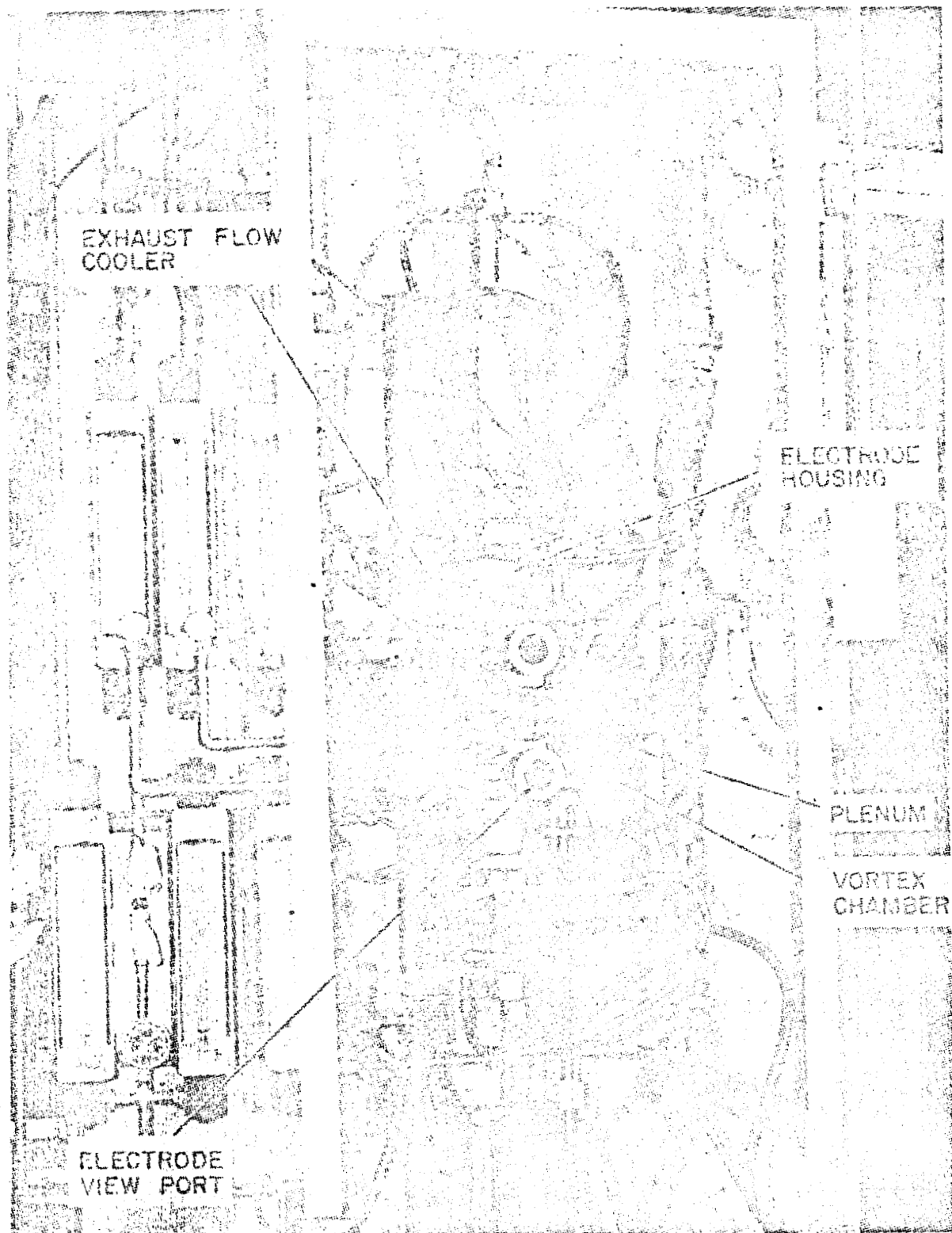


Figure 3b Tandem Gerdien Free Jet Arc Facility  
Showing Arc Heater Equipment

UNCLASSIFIED

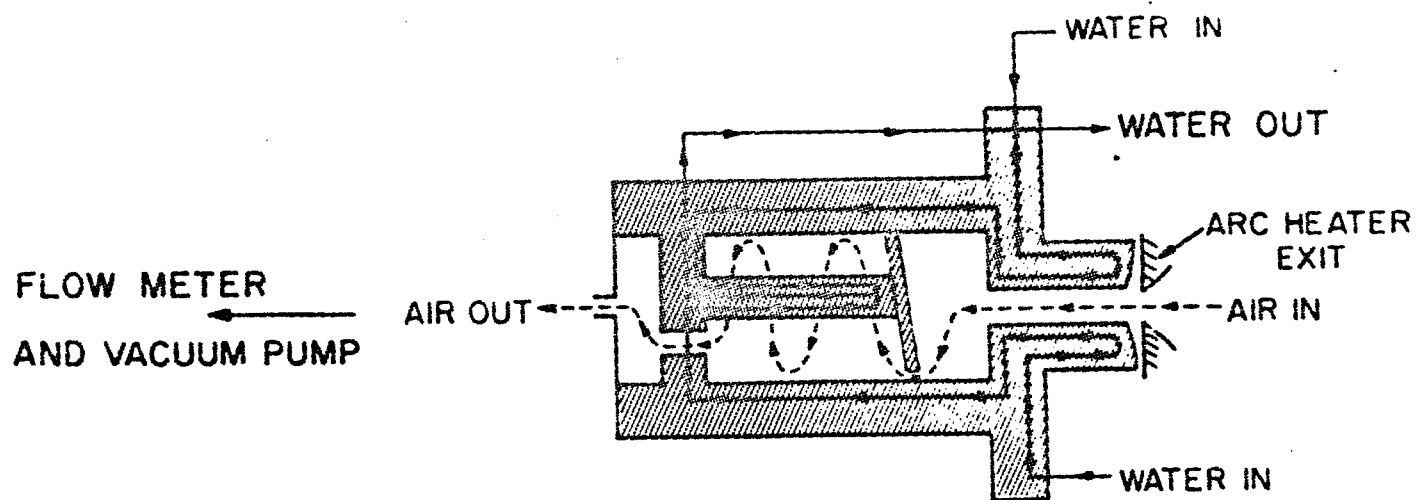
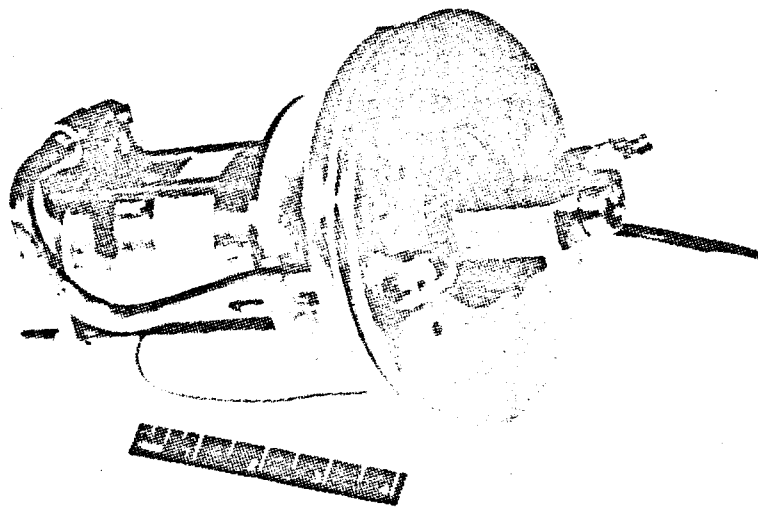


FIGURE 4 TOTAL ENTHALPY CALORIMETER FOR ARC TUNNEL

UNCLASSIFIED



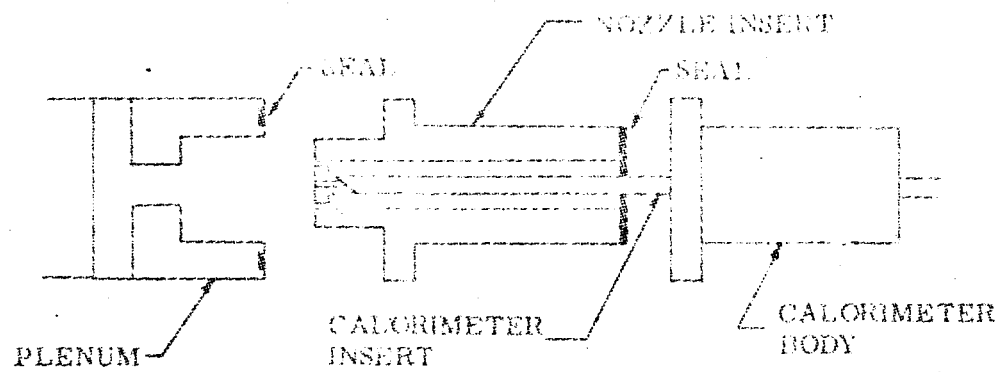


Figure 5 Total Enthalpy Calorimeter Tandem Gerdien Free Jet Arc

UNCLASSIFIED

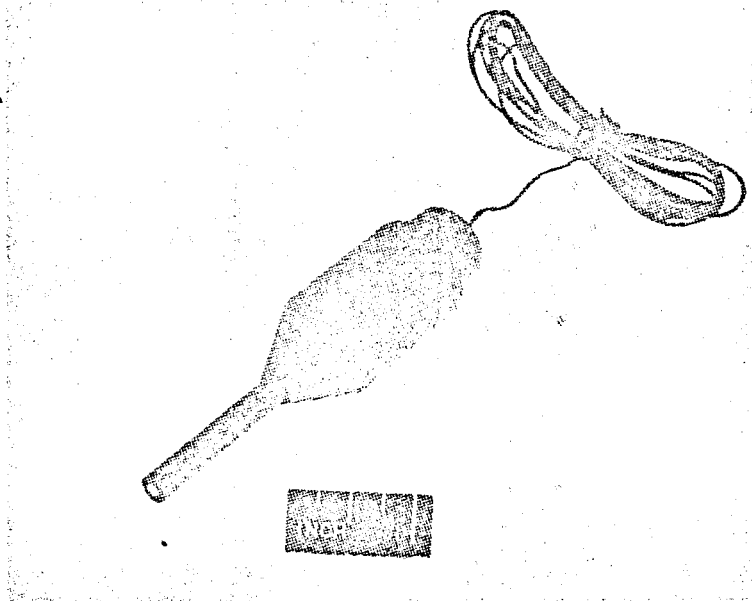


FIGURE 6 TYPICAL MASS TRANSFER MODEL CALORIMETER

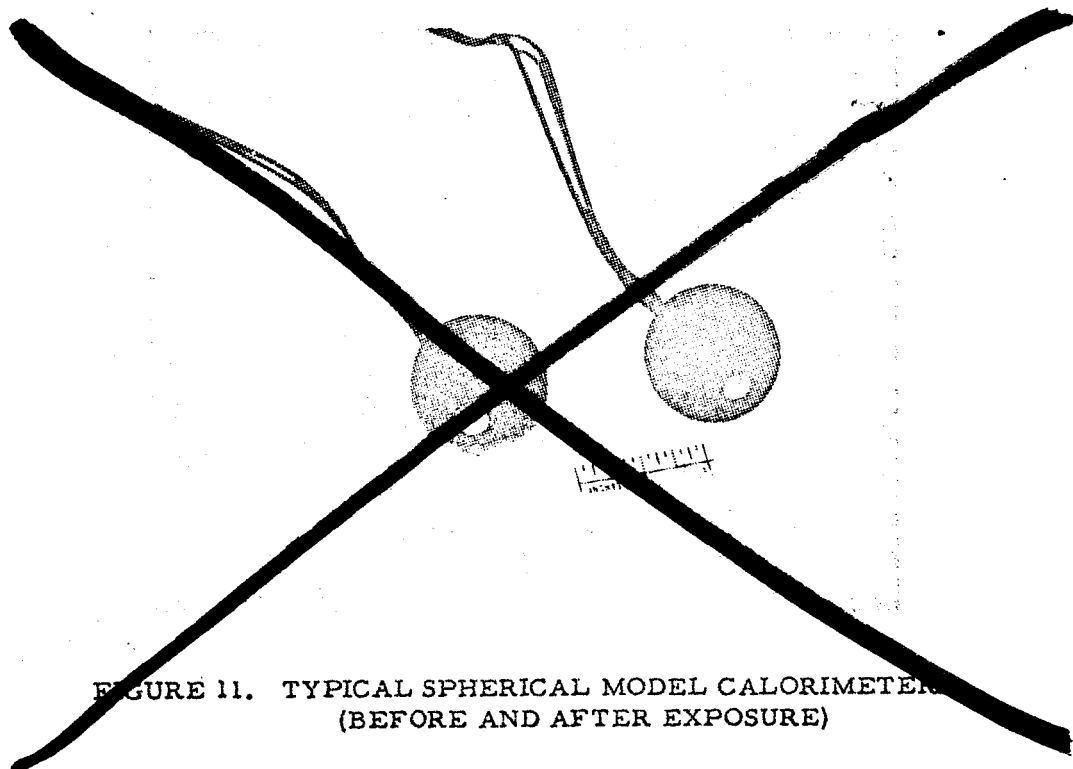


FIGURE 11. TYPICAL SPHERICAL MODEL CALORIMETER  
(BEFORE AND AFTER EXPOSURE)

UNCLASSIFIED

UNCLASSIFIED

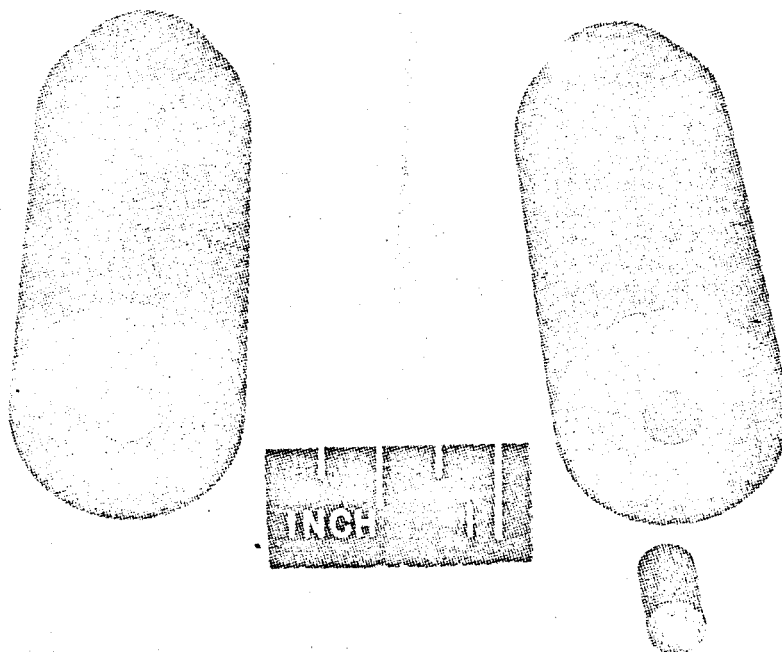


Figure 7a-1 MASS RATE SPECIMEN, 1.0" DIAMETER

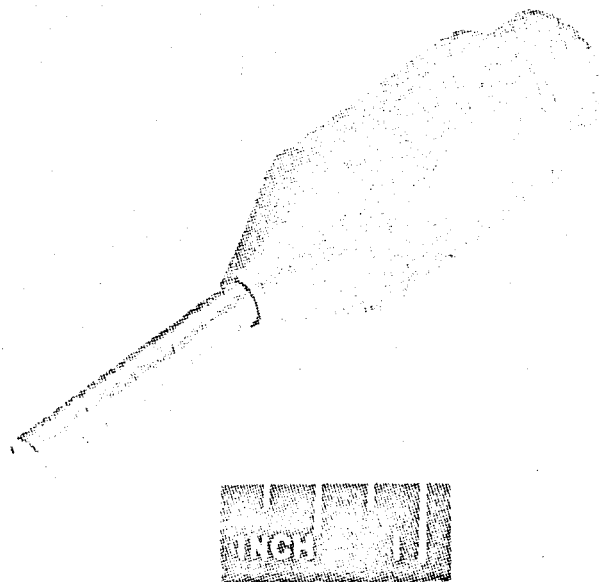


Figure 7a-2 MASS RATE SPECIMEN, 1/4" DIAMETER

UNCLASSIFIED

UNCLASSIFIED

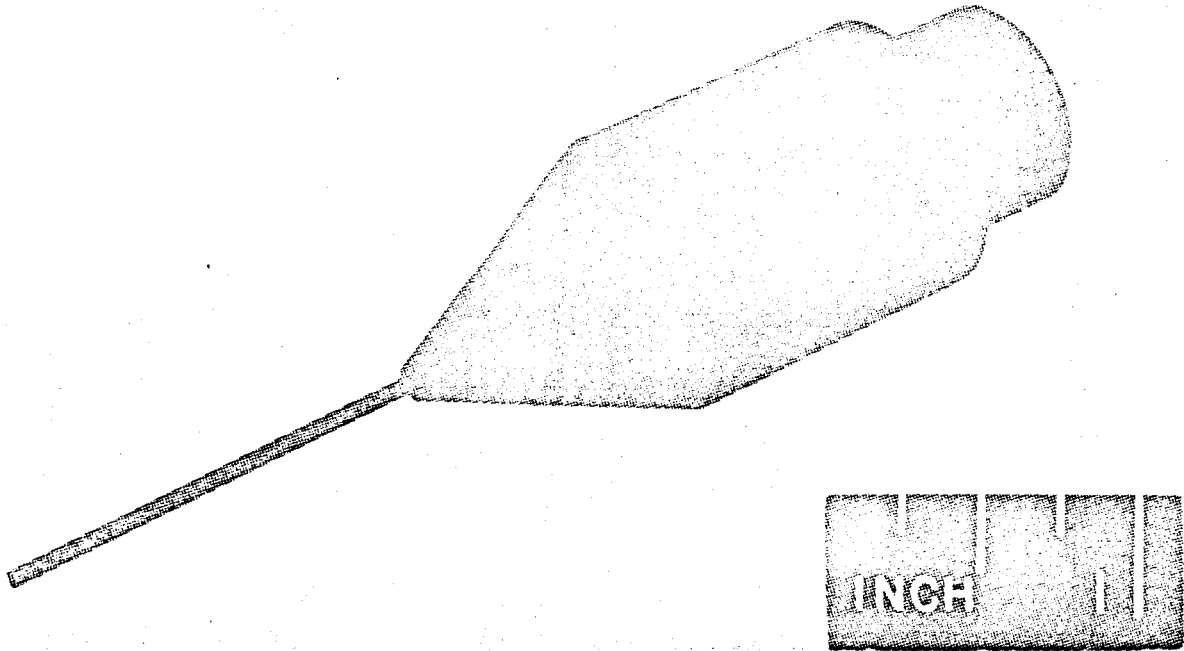


Figure 7a-3 MASS RATE SPECIMEN, 1/16" DIAMETER

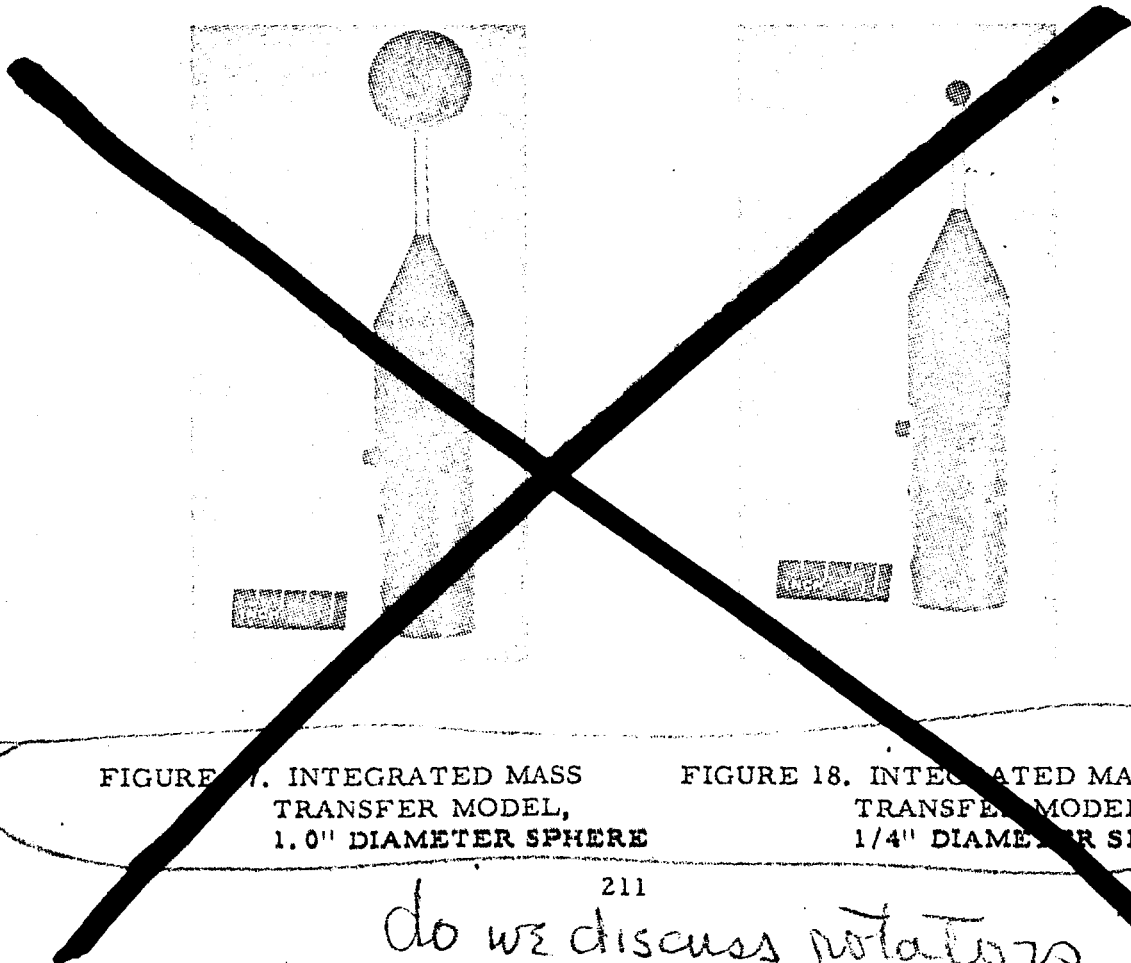


FIGURE 17. INTEGRATED MASS  
TRANSFER MODEL,  
1.0" DIAMETER SPHERE

FIGURE 18. INTEGRATED MASS  
TRANSFER MODEL,  
1/4" DIAMETER SPHERE

211

do we discuss rotations

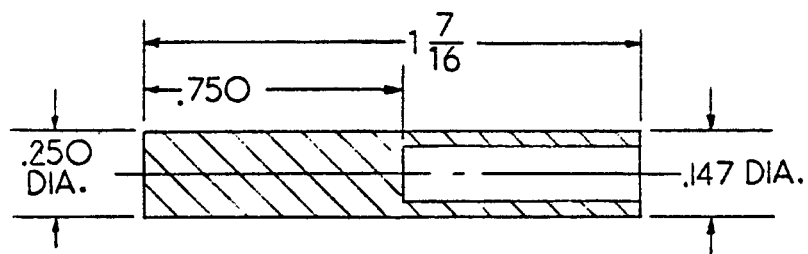
UNCLASSIFIED

UNCLASSIFIED

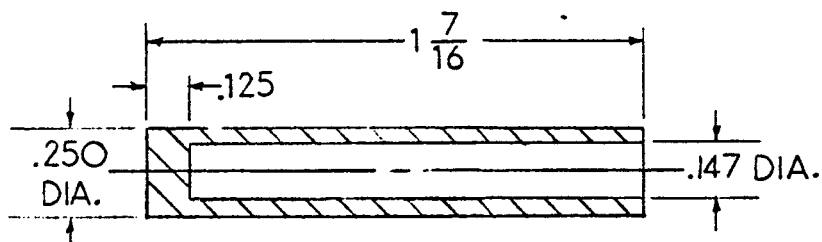
## MODIFICATIONS OF ATJ GRAPHITE SPECIMENS

$\frac{1}{4}$  IN. DIA. MODELS

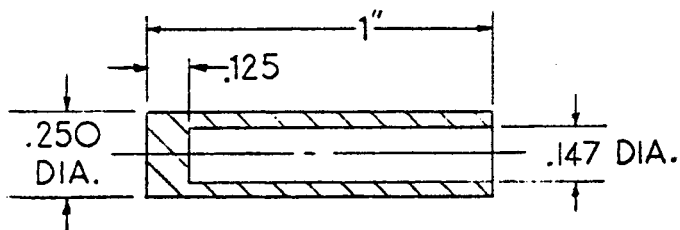
ITEM 17 FIG.12



a



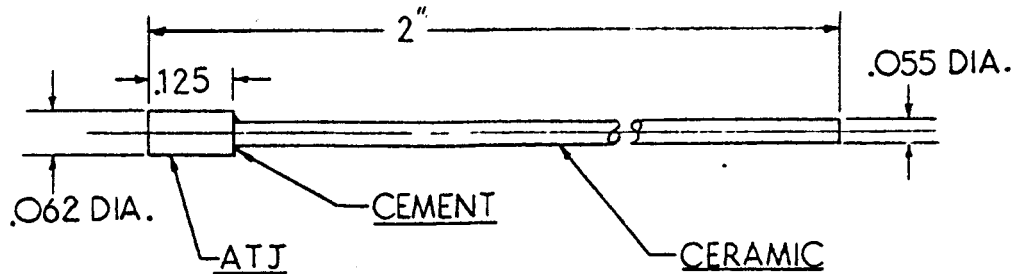
b



c

$\frac{1}{16}$  IN. DIA. MODEL

ITEM 21 FIG.12



d

FIGURE 7b

UNCLASSIFIED

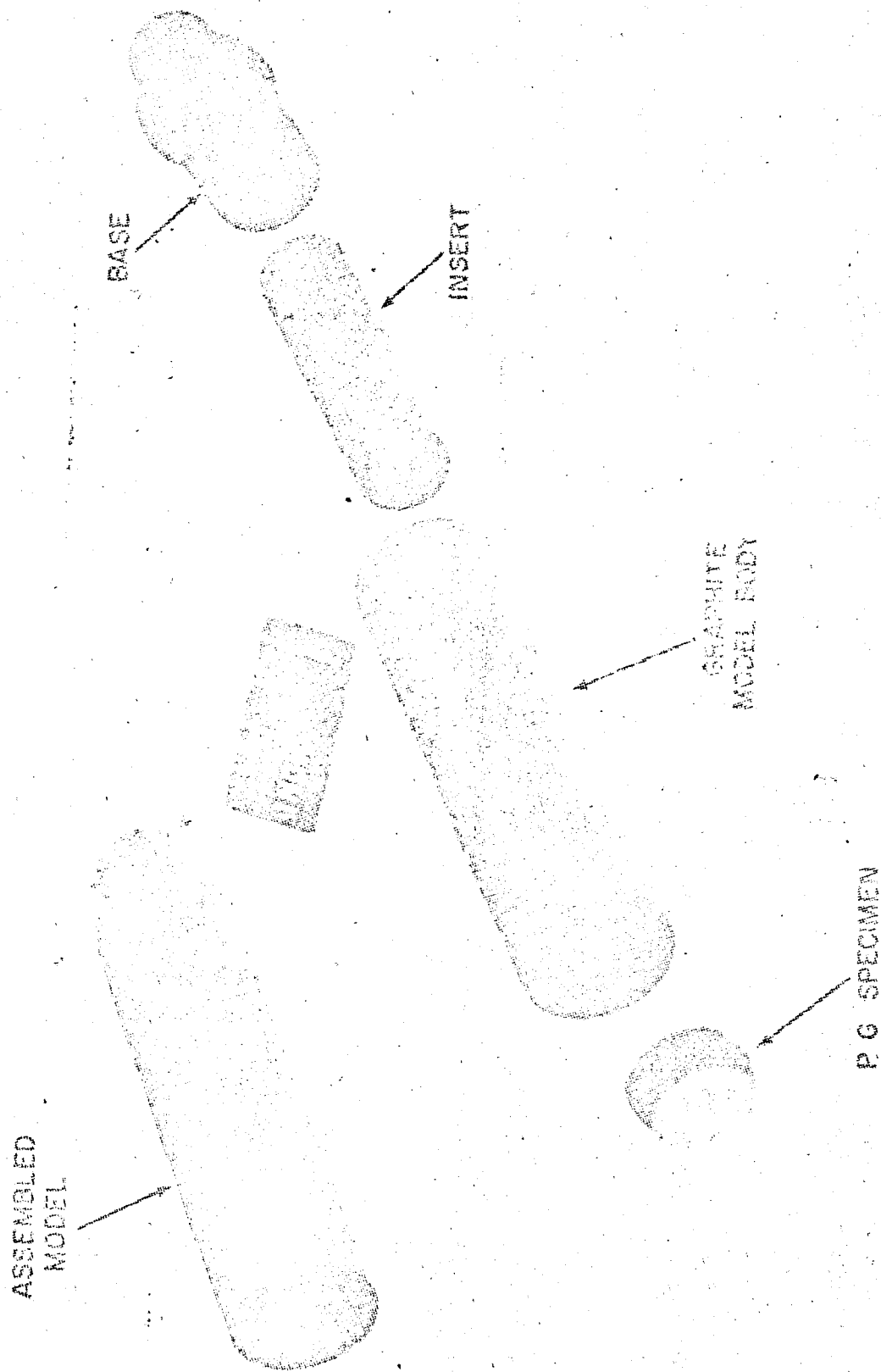


Figure 7c Model used in five jet tests

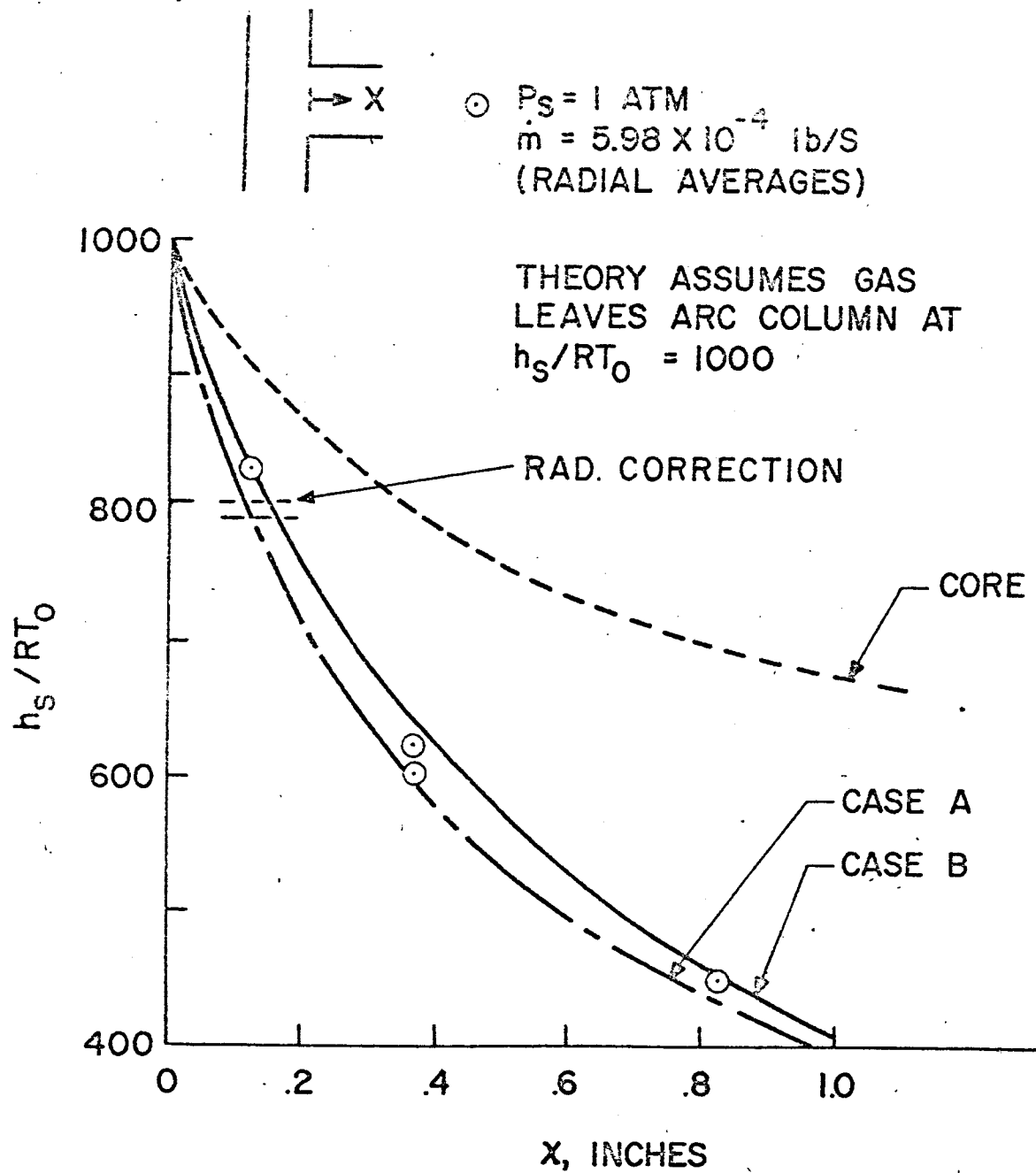


Figure 8. Comparison of experimental and theoretical stagnation enthalpy levels

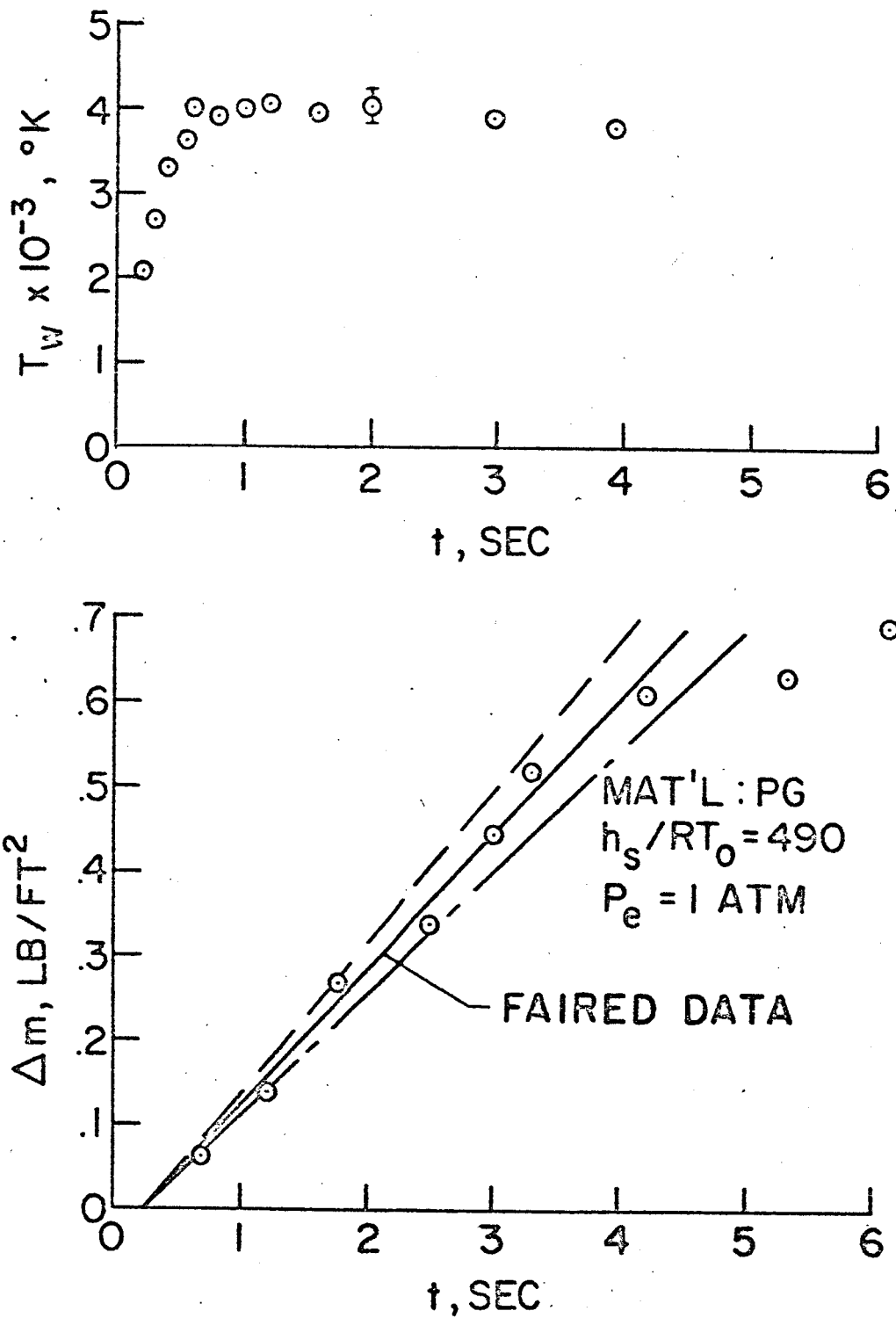


Figure 9a Surface temperature and mass loss measurements for free jet tests of pyrolytic graphite, - high enthalpy



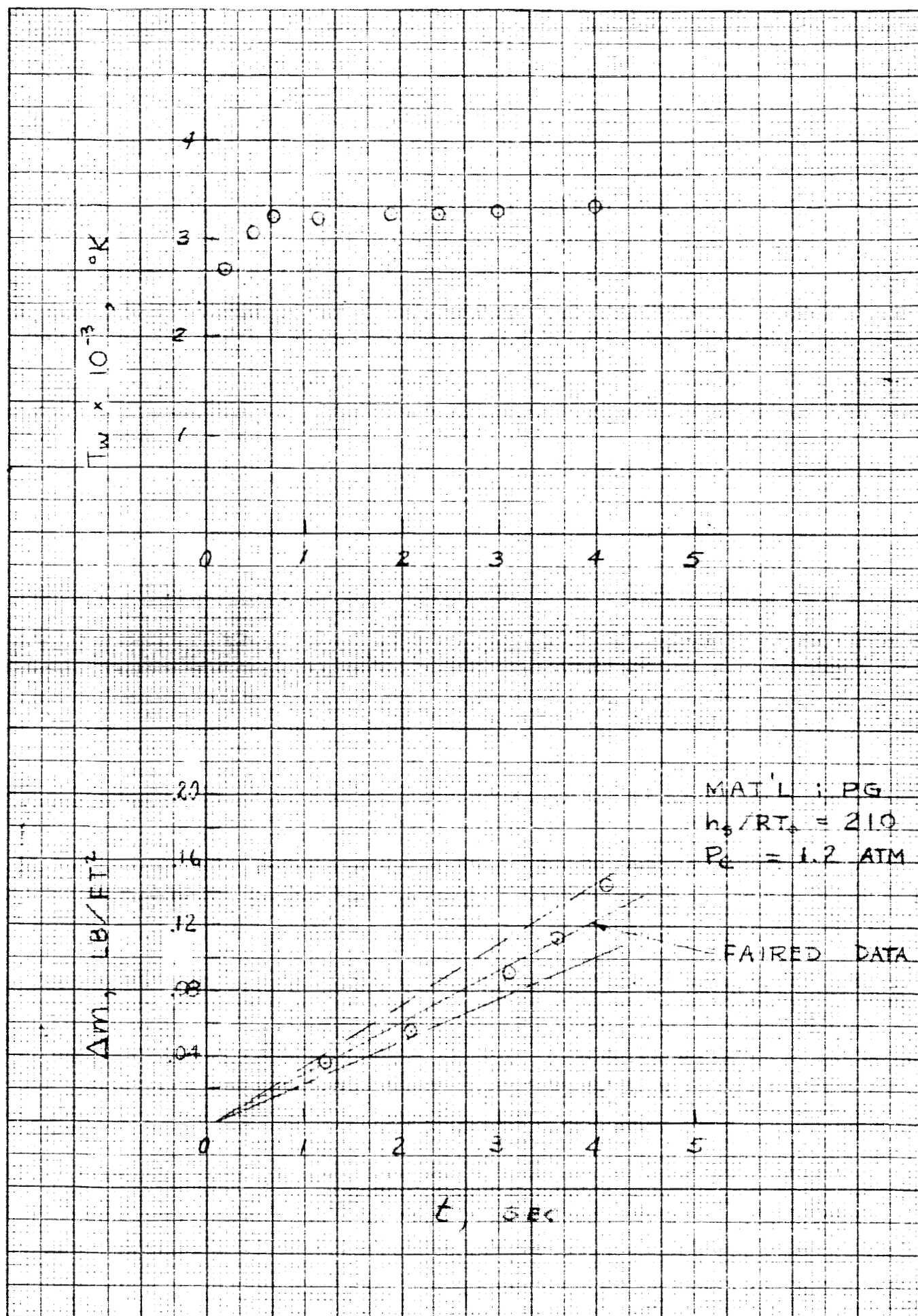
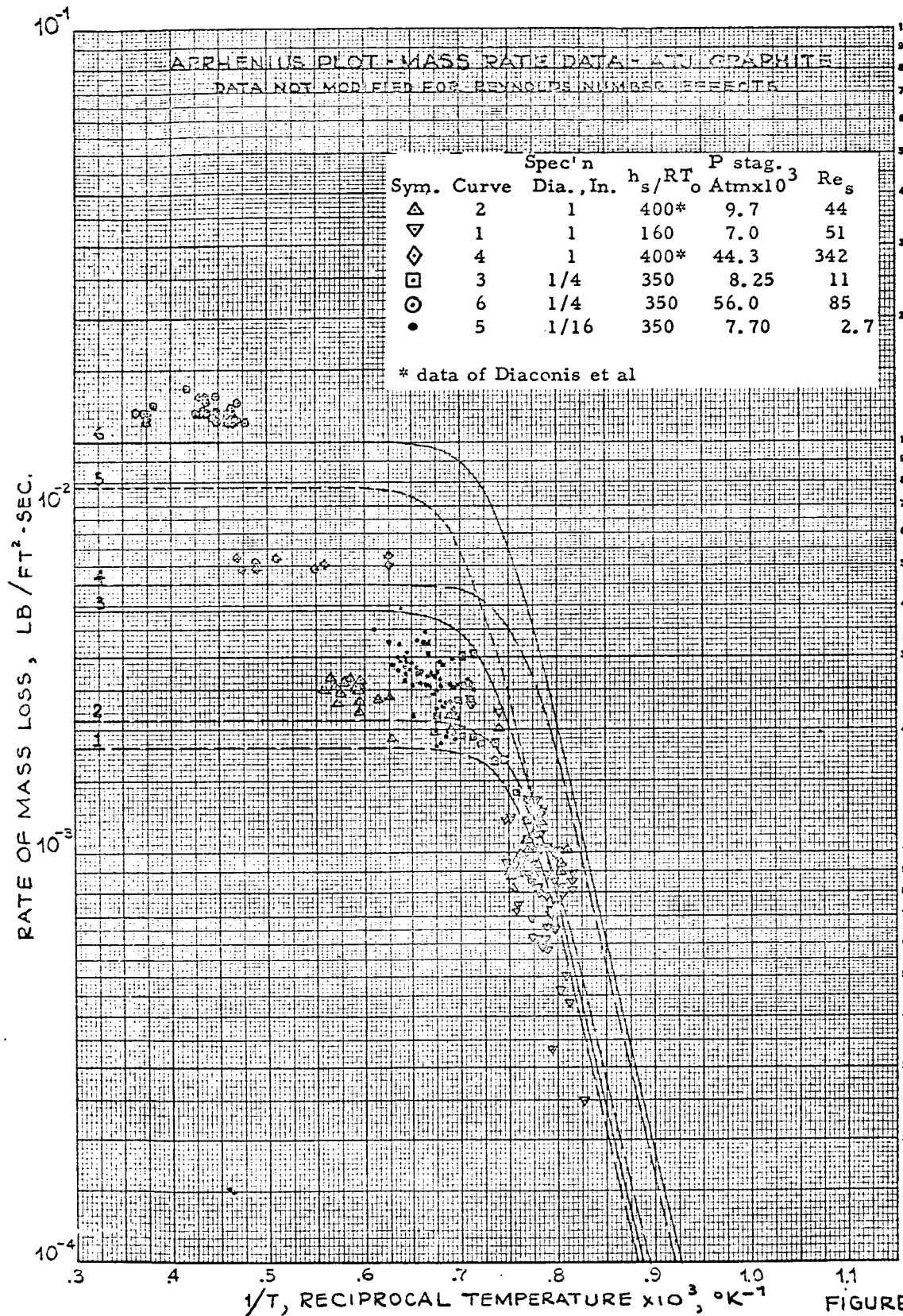


Figure 9b - Surface temperature and mass loss measurements for free jet tests of pyrolytic graphite - low enthalpy

UNCLASSIFIED



UNCLASSIFIED

UNCLASSIFIED

# FLOW REGIME CORRELATION FUNCTION

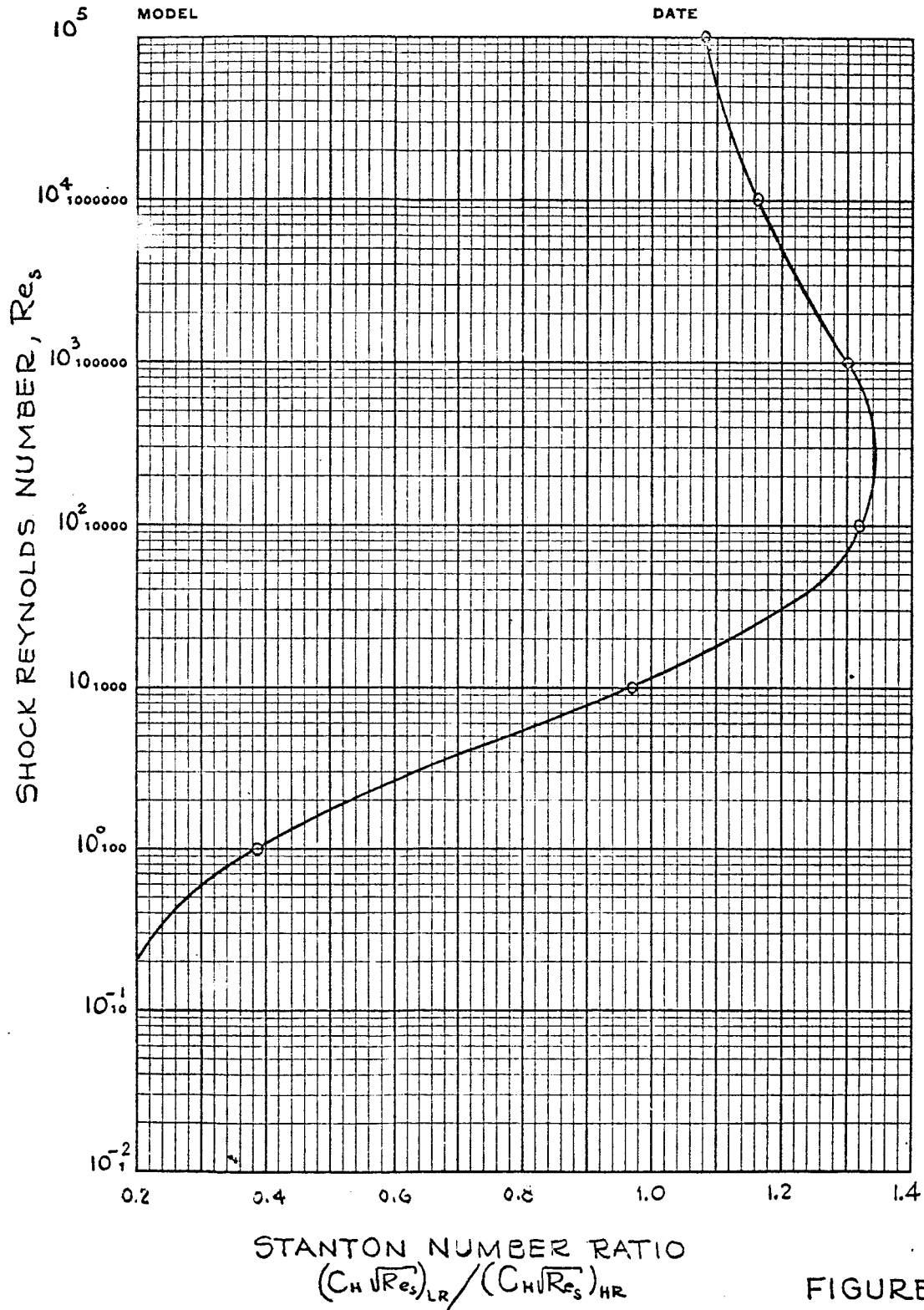


FIGURE 12

UNCLASSIFIED

UNCLASSIFIED

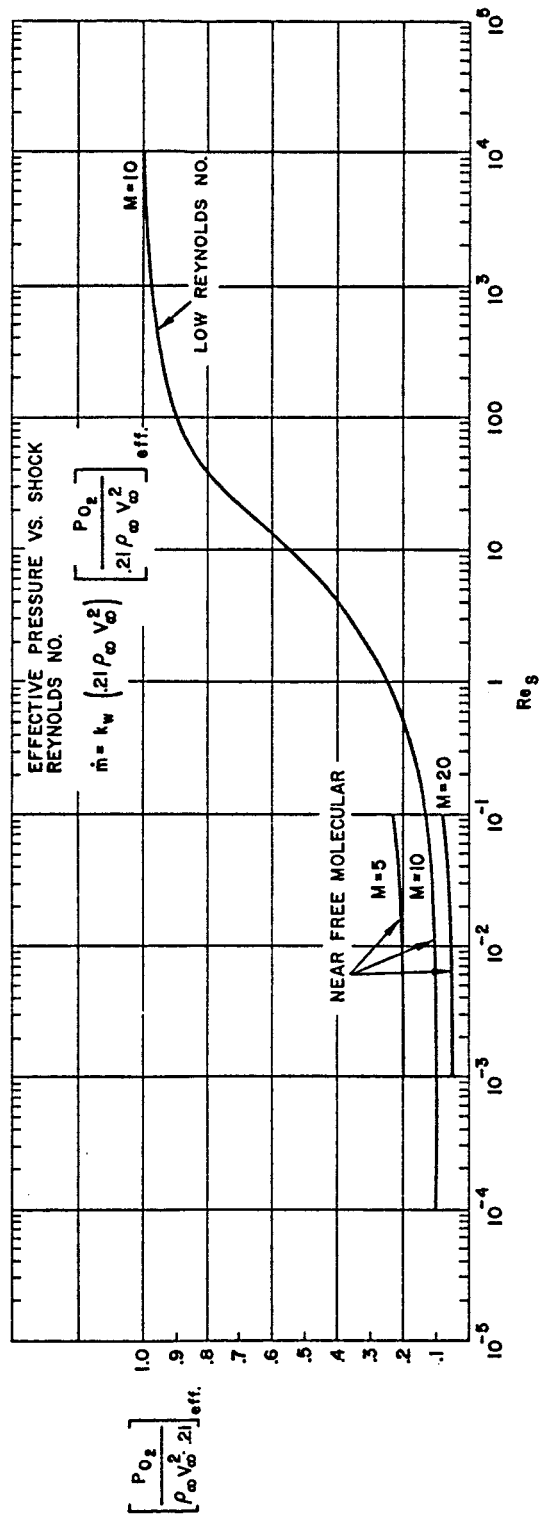


FIGURE 13

UNCLASSIFIED

UNCLASSIFIED

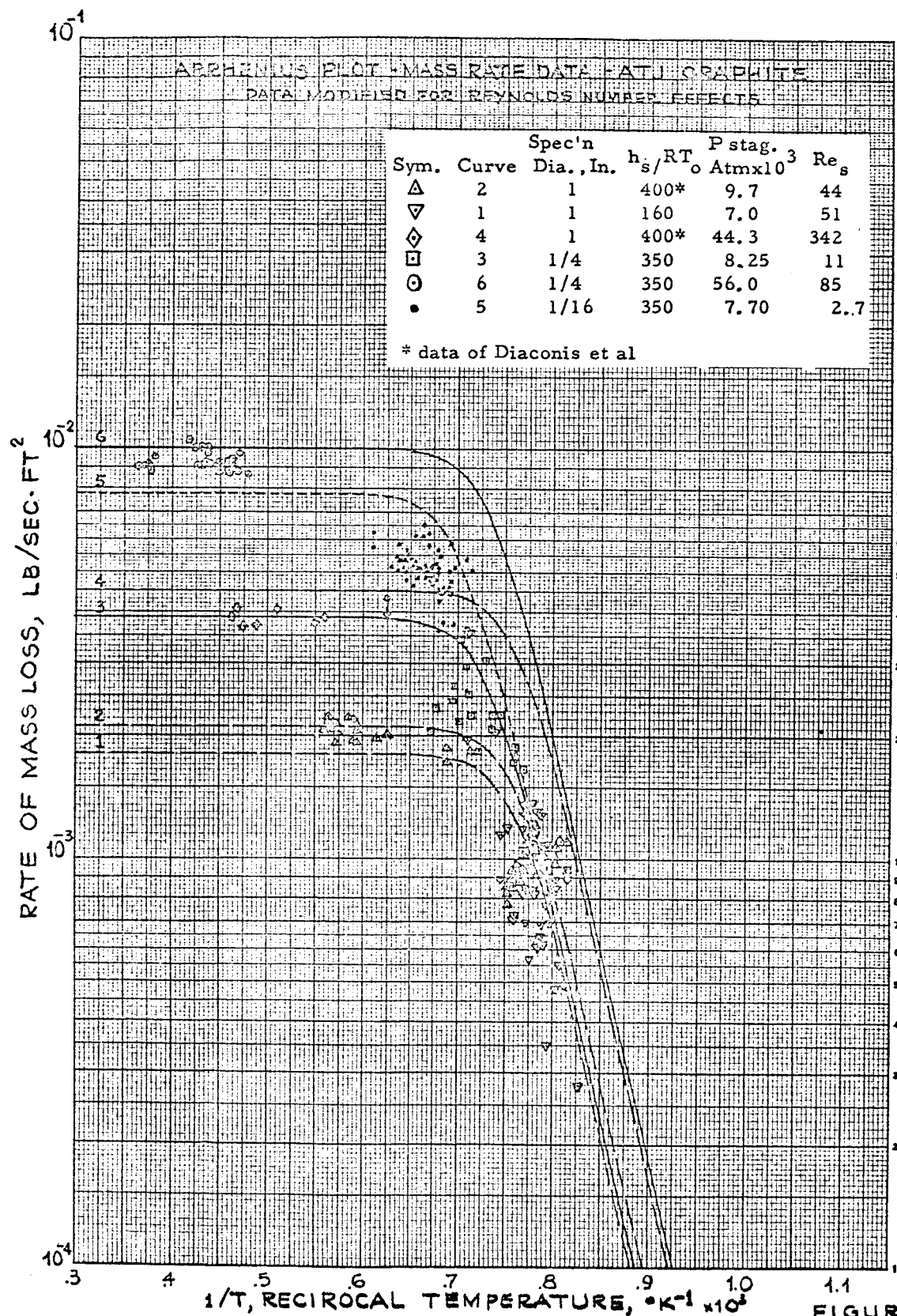


FIGURE 14

UNCLASSIFIED

# OXIDATION MASS RATE VS. SURFACE TEMPERATURE FOR ATJ GRAPHITE

Data Obtained one-dimensionally from Axially  
Oriented, Flat Ended Cylinder Specimens in  
Low Density Hypersonic Air Flows; Theory  
Curves for Continuum Adjusted to Correlate  
Directly with Experimental Data

$$\frac{\dot{m}}{A} \sqrt{\frac{R_s}{P_s}} = \frac{1.6}{\sqrt{P_s}} \left( \frac{R_s}{P_s} \right)^{1/2} \text{ LB/FT}^2 \cdot \text{SEC} \cdot \text{ATM}^{1/2} \times 10^3$$

$$\frac{\dot{m}}{A} \sqrt{\frac{R_s}{P_s}} = \frac{k_0 f_2 e^{-E/RT}}{[1/R_s + (G_1 k_0 / f_1 C)^2 e^{-2E/RT}]^{1/2}}$$

WHERE  $G_1 = 6.2 \times 10^{-3} \text{ LB/FT}^{3/2} \cdot \text{SEC} \cdot \text{ATM}^{1/2}$

$k_0 = 4.42 \times 10^3 \text{ LB/FT}^2 \cdot \text{SEC} \cdot \text{ATM}^{1/2}$

$E = 44000 \text{ CAL}$

$R = 1.987 \text{ CAL/}^\circ\text{K}$

$f_1$  = MODIFYING FACTOR FOR  $R_{s2}$  IN  
DIFFUSION CONTROLLED REGIME

$f_2$  = MODIFYING FACTOR FOR  $R_{s2}$  IN  
REACTION CONTROLLED REGIME

TEMPERATURE,  $^\circ\text{F}$

TEMPERATURE,  $^\circ\text{C}$



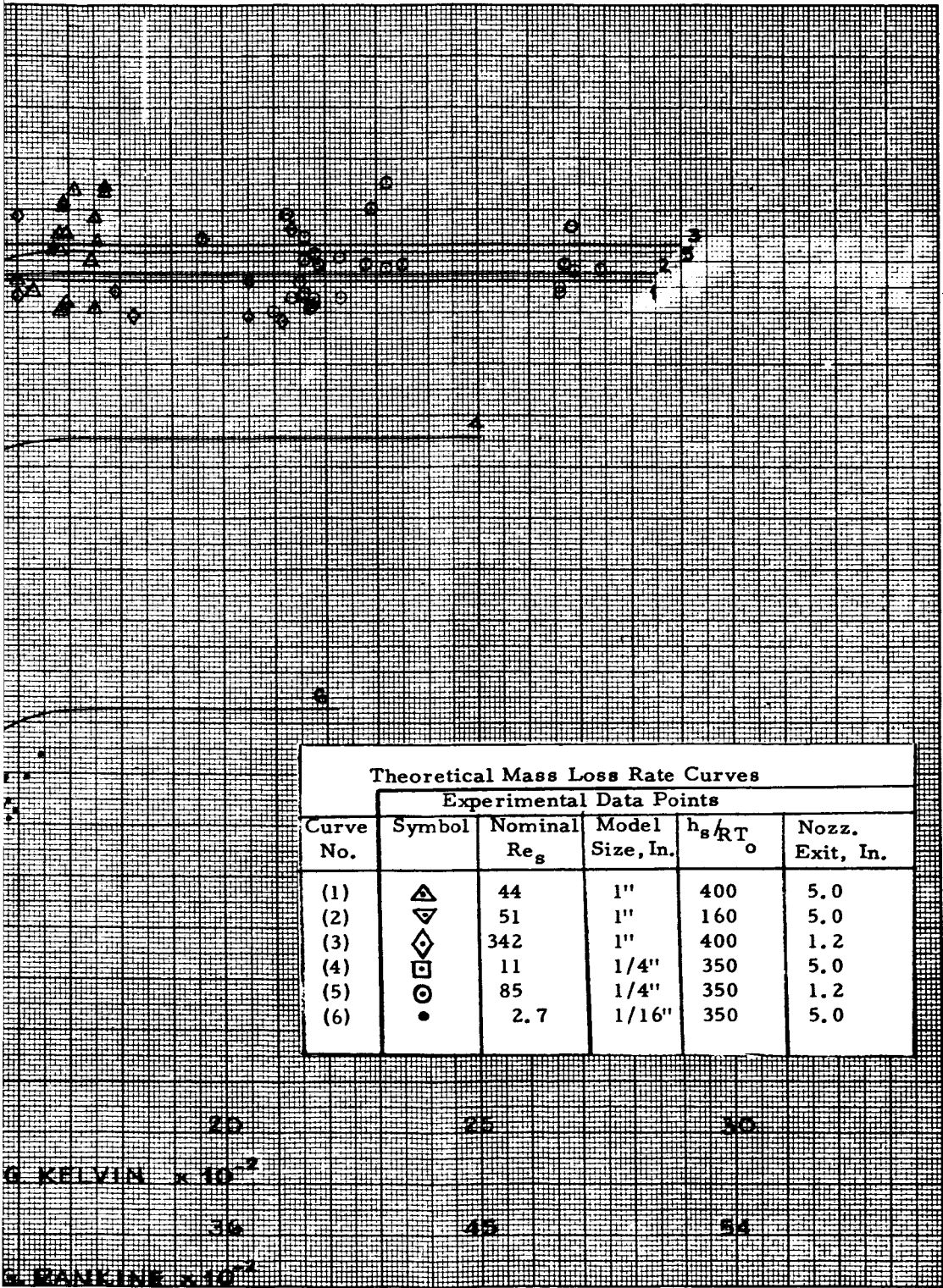


FIGURE 15

# OXIDATION MASS RATE VS. SURFACE TEMPERATURE FOR ATJ GRAPHITE

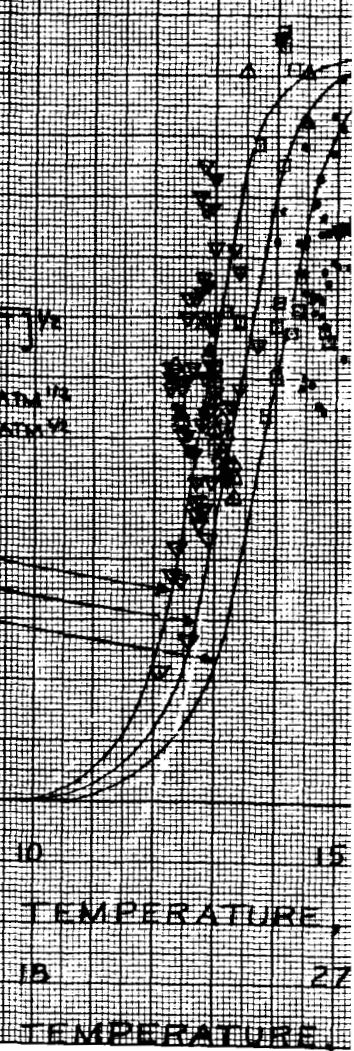
Data Obtained one-dimensionally from Axially  
Oriented Flat Ended Cylinder Specimens in  
Low Density Hypersonic Air Flows; Data Ad-  
justed for Correlation with Continuum Theory.

$$\dot{m}_w \sqrt{\frac{R_g}{P_0}} = \frac{LB}{FT^{3/2}} - SEC - ATM^{1/2} \times 10^3$$

$$\dot{m}_w \sqrt{\frac{R_g}{P_0}} = \frac{K_0 e^{-E/RT}}{[1/R_0 + (K_0/d)^2 e^{-2E/RT}]^{1/2}}$$

WHERE  $C = 6.2 \times 10^{-2}$  LB/FT<sup>3/2</sup> - SEC - ATM<sup>1/2</sup>  
 $K_0 = 4.42 \times 10^5$  LB/FT<sup>2</sup> - SEC - ATM<sup>1/2</sup>  
 $E = 44000$  CAL.  
 $R = 1.987$  CAL/°K

COMPUTED FROM THEORY (d = 1/4")  
WHERE  $R_0 = \left(\frac{2.46}{24}\right)d$   
d = 1/8"  
d = 1/16"





UNCLASSIFIED

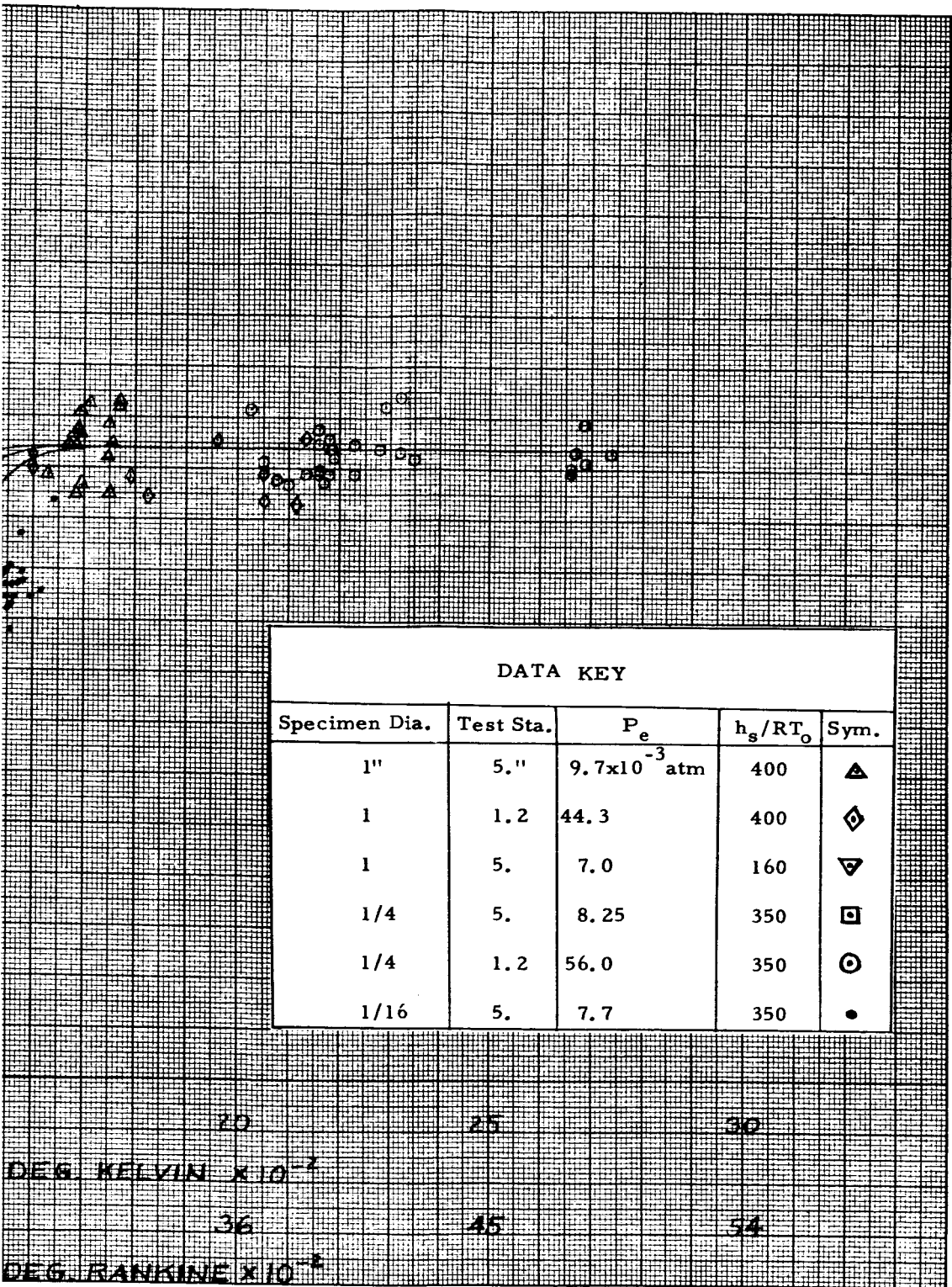


FIGURE 16

✓

UNCLASSIFIED

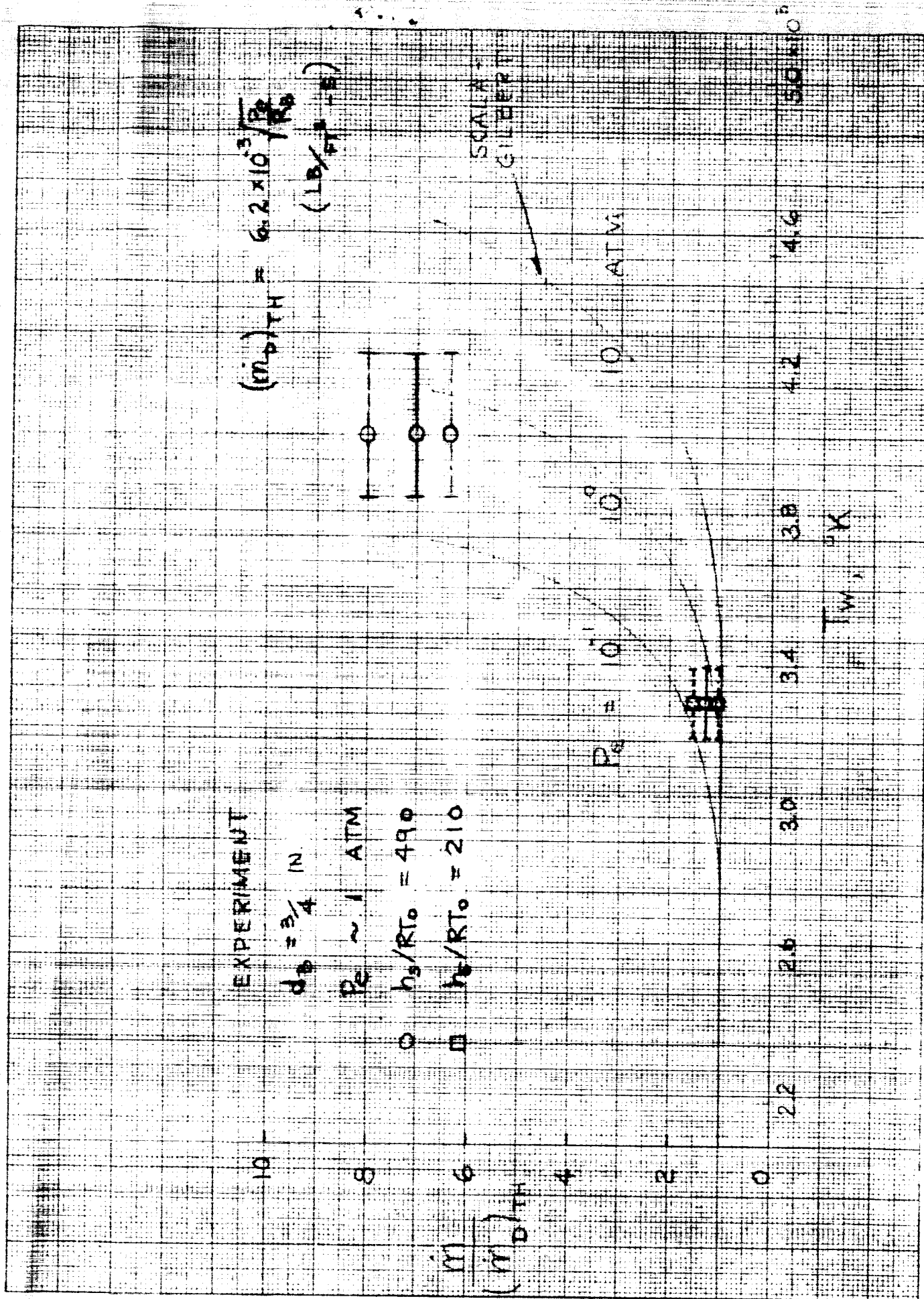
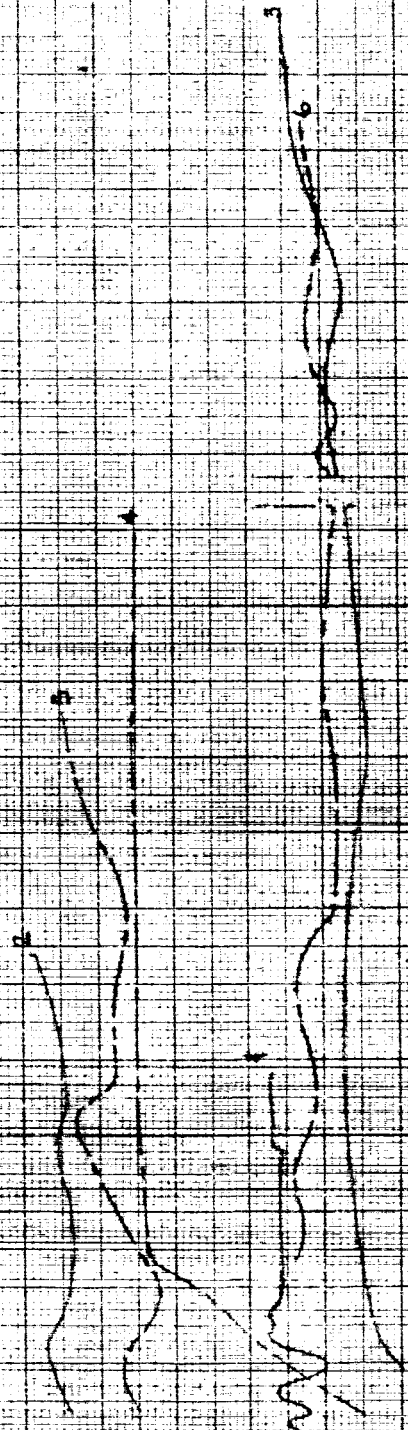


Fig. 17 COMPARISON OF EXPERIMENT WITH  
THEORY - PYROLYTIC GRAPHITE

# RANDOM SELECTION OF TYPICAL SURFACE TEMPERATURES CYLINDRICAL MASS RATE SPECIMENS

TEMPERATURE  
°C  
45  
24



CURVE NO.	RUN NO.	MATL	NOMINAL DIA. IN.	NOZZLE DIA. IN.
1	519	ATI	350	1/16
2	497	"	"	1/4
3	632	"	160	1
				5.0
				1.2
				5.0

TIME - SECONDS